Published in final edited form as:
Geochim Cosmochim Acta. 2015 April 15; 155: 122–153. doi:10.1016/j.gca.2015.02.004.

Diverse impactors in Apollo 15 and 16 impact melt rocks: evidence from osmium isotopes and highly siderophile elements

Jingao Liu[a,b,*], **Miriam Sharp**[a], **Richard D. Ash**[a], **David A. Kring**[c], **Richard J. Walker**[a]

[a]Department of Geology, University of Maryland, College Park MD 20742 USA

[b]Department of Earth and Atmospheric Sciences, University of Alberta, 1-26 Earth Sciences Building, Edmonton AB T6G 2E3 Canada

[c]Center for Lunar Science and Exploration, Lunar and Planetary Institute, Universities Space Research Association, 3600 Bay Area Boulevard, Houston, Texas 77058, USA

Abstract

Concentrations of highly siderophile elements (HSE) and $^{187}Os/^{188}Os$ isotopic compositions for eleven impact related rocks from the Apollo 15 and 16 landing sites are reported and combined with existing geochronological data to investigate the chemical nature and temporal changes in the large impactors implicated in the formation of the lunar basins. Data for the samples all define linear trends on plots of HSE versus Ir concentrations, whose slopes likely reflect the relative HSE compositions of the dominant impactors that formed the rocks.

The inferred Imbrium basin impactor that generated Apollo 15 impact melt rocks 15445 and 15455 was characterized by modestly suprachondritic $^{187}Os/^{188}Os$, Ru/Ir, Pt/Ir and Pd/Ir ratios. Diverse impactor components are revealed in the Apollo 16 impact melt rocks. The $^{187}Os/^{188}Os$ and HSE/Ir ratios of the impactor components in melt rocks 60635, 63595 and 68416, with reported ages < 3.84 Ga, are within the range of chondritic meteorites, but slightly higher than ratios characterizing previously studied granulitic impactites with reported ages > 4.0 Ga. By contrast, the impactor components in melt rocks 60235, 62295 and 67095, with reported ages of ~3.9 Ga, are characterized by suprachondritic $^{187}Os/^{188}Os$ and HSE/Ir ratios similar to the Apollo 15 impact melt rocks, and may also sample the Imbrium impactor. Three lithic clasts from regolith breccias 60016 and 65095, also with ~3.9 Ga ages, contain multiple impactor components, of which the dominant composition is considerably more suprachondritic than those implicated for Imbrium and Serenitatis (Apollo 17) impactors. The dominant composition recorded in these rocks was most likely inherited from a pre-Imbrium impactor. Consideration of composition versus age relations among lunar impact melt rocks reveals no discernable trend.

Virtually all lunar impact melt rocks sampled by the Apollo missions, as well as meteorites, are characterized by $^{187}Os/^{188}Os$ and HSE/Ir ratios that, when collectively plotted, define linear trends ranging from chondritic to fractionated compositions. The impact melt rocks with HSE signatures within the range of chondritic meteorites are interpreted to have been derived from impactors that had HSE compositions similar to known chondrite groups. By contrast, the impact melt rocks

[*]Correspondence author: jingao@ualberta.ca, Department of Earth and Atmospheric Sciences, University of Alberta, 1-26 Earth Sciences Building, Edmonton AB T6G 2E3 Canada.

with non-chondritic relative HSE concentrations could not have been made by mixing of known chondritic impactors. These signatures may instead reflect contributions from early solar system bodies with bulk chemical compositions that have not yet been sampled by primitive meteorites present in our collections. Alternately, they may reflect the preferential incorporation of evolved metal separated from a fractionated planetesimal core.

Pre-3.9 Ga ages for at least some impactor components with both chondritic and fractionated HSE raise the possibility that the bulk of the HSE were added to the lunar crust prior to the later-stage basin-forming impacts, such as Imbrium and Serenitatis, as proposed by Fischer-Gödde and Becker (2012). For this scenario, the later-stage basin-forming impacts were more important with respect to mixing prior impactor components into melt rocks, rather than contributing much to the HSE budgets of the rocks themselves.

1. INTRODUCTION

The Moon provides a record of the end stages of major planetary accretion to the inner solar system in the form of large impact basins. The observed basin-forming impacts have been interpreted by some to be a result of a putative late heavy bombardment of the inner solar system that occurred between approximately 4.1 and 3.8 billion years ago (Tera et al., 1974; Ryder, 2002; Norman et al., 2006). However, the timing and source of the impactors have been controversial. Regardless of timing, the basin-forming impact events generated voluminous impact melt rocks and breccias that are typically enriched, relative to pristine lunar crustal rocks, in impactor-derived highly siderophile elements (HSE: here including Re, Os, Ir, Ru, Pt, and Pd) (e.g., Anders et al., 1973; Morgan et al., 1974; Higuchi and Morgan, 1975; Wasson et al., 1975; Gros et al., 1976; Hertogen et al., 1977; Korotev, 1987, 1994; Norman et al., 2002; Puchtel et al., 2008; Fischer-Gödde and Becker, 2012; Sharp et al., 2014). Consequently, impact melt rocks can provide important information about the relative concentrations of the HSE present in impactors involved in basin-forming events on the Moon, and by inference, contemporaneous impacts occurring on the Earth and other terrestrial planets.

Studies of Apollo and meteoritic lunar impact melt rocks have reported that, whereas some have HSE characteristics that are well within the range of chondritic meteorites, others are characterized by suprachondritic $^{187}Os/^{188}Os$ (a proxy for long-term Re/Os evolution), Ru/Ir, Pt/Ir, Au/Ir and Pd/Ir ratios, as well as subchondritic Os/Ir ratios (Morgan et al., 1972, 1974; Korotev, 1994; James et al., 2002; Norman et al., 2002; Puchtel et al., 2008; Fischer-Gödde and Becker, 2012; Sharp et al., 2014). The non-chondritic HSE ratios have commonly been interpreted to reflect either the participation of impactors with bulk compositions outside of the range of presently sampled chondrites (Morgan et al., 1974; Norman et al., 2002; Puchtel et al., 2008; Sharp et al., 2014), or impactors with HSE that were variably fractionated as a result of metal-silicate or solid metal-liquid metal processing on their respective parent bodies (Goldstein et al., 1972; Morgan et al., 1972; Reed and Taylor, 1974; Korotev, 1994; James et al., 2002; Fischer-Gödde and Becker, 2012).

Numerous questions remain regarding the interpretation of HSE signatures in lunar impact melt rocks. How much did processes occurring within an evolving melt sheet modify the

absolute and relative concentrations of HSE? For a given impact melt rock, what was the proportion of HSE derived from earlier impacts relative to the HSE added by the basin-forming event that purportedly created the melt rock? Related to this, can the HSE signatures of different generations of impactors be discriminated in a single rock? Where there are distinct HSE signatures present in different impact melt rocks from a given site, do the differences reflect chemical heterogeneities present in a single, basin-forming impactor, or are they the result of multiple smaller, crater-forming events involving chemically diverse impactors (e.g., Korotev, 1994)? Finally, are there unifying characteristics in the HSE signatures of different impact melt rocks from different sites that may argue for the global mixing of impactors that can potentially account for most of the chemical variations observed? For example, Fischer-Gödde and Becker (2012) concluded that linear trends observed on plots of HSE ratios from different lunar sites are indicative of the global mixing of two major HSE-rich components, one that was much like carbonaceous chondrites, and the other a metal component that formed as part of a crystallizing planetesimal core.

Here we report HSE concentration and Os isotopic data for eleven lunar impact-related melt rocks; two from the Apollo 15 site (melt rocks 15445 and 15455), and nine from the Apollo 16 site (two lithic clasts extracted from regolith breccia 60016, one lithic clast extracted from regolith breccia 65095, and six bulk impact melt rocks 60235, 60635, 62295, 63549, 67095 and 68416). The main objective of this work is to investigate the chemical nature of impactors contributing HSE to the Apollo 15 and 16 impact melt rocks. The data are combined with age data reported for the same rocks, and compared with HSE and age data for lunar impact rocks from other sampling sites (Norman et al., 2002; Puchtel et al., 2008; Fischer-Gödde and Becker, 2012; Sharp et al., 2014), allowing re-assessment of the extent of chemical homogeneity/heterogeneity among impactors involved in different basin-forming events, and placing constraints on the source of the impactors.

2. SAMPLES

Brief petrographic descriptions and a review of existing age data for Apollo 15 and 16 impact melt rocks are summarized in Table 1. Also included are age data for other lunar impact melt rocks for which complementary HSE concentrations and Os isotopic compositions exist.

2.1. Apollo 15 impact melt rocks

The Apollo 15 landing site is located on Hadley Delta, the smooth basaltic lava plain, east of the sinuous Hadley Rille lava depression, on the arcuate eastern rim of the Imbrium basin (Fig. 1a). To the east of Hadley Delta are the Montes Apennines, forming an arc of rugged massifs along the margin of the Imbrium basin (*Apollo 15 Preliminary Science Report, 1972*).

Samples 15445 and 15455, examined here, were collected from the rim of the Spur Crater (Fig. 1a), and have been described as recrystallized impact melt rocks containing shocked clasts of plutonic rocks (Ryder and Bower, 1977). Based upon field locations, Ryder and Bower (1977) and Ryder and Wood (1977) concluded that both samples represent ejecta from the Imbrium basin-forming event. The incorporated clasts include norites, anorthosites

and spinel troctolites. Several of the clasts have been dated at ~4.3 to 4.5 Ga using the Rb-Sr and Sm-Nd dating methods, and may represent some of the oldest lunar materials sampled by the Apollo missions (Shih et al., 1993). The younger, dark matrix material in both rocks consists of fine-grained plagioclase, olivine and opaque minerals. The matrix is generally free of fragments from the large clasts. The matrix and clasts for 15455 have an average ^{40}Ar-^{39}Ar age of ~3.9 Ga that has been interpreted to reflect the age of the Imbrium impact event (Alexander and Kahl, 1974; Bernstein, 1983; Shih et al., 1993), and is broadly consistent with more recent reports of ages of 3.91 to 3.94 Ga for the formation of the Imbrium basin (Gnos et al., 2004; Liu et al., 2012; Merle et al., 2014). Prior studies have reported that small aliquots of bulk samples of these rocks contain HSE concentrations that are typical for lunar impact melt rocks, with Ir ranging from 2.5 to 6.2 ng/g and from 2 to 7 ng/g, for samples 15445 and 15455, respectively (Ganapathy et al., 1973; Gros et al., 1976; Lindstrom et al., 1988). By contrast, separated noritic and troctolitic clasts contain much lower concentrations of HSE, with Ir concentrations of ≤ 0.02 ng/g (Ganapathy et al., 1973; Warren and Wasson, 1979; 1980). The comparatively high HSE concentrations in the matrix of 15445 and 15455 support the interpretation that these rocks were produced by a basin-forming impact, rather than a volcanic process.

We were allocated ~2 g each of dark splits 15445,229 and 15455,326. Both samples were coherent and dense, with some vesicles in which metal grains and troilites were observed. For this study, we subdivided and analyzed 10 and 11 subsamples of 15445 and 15455, respectively, for HSE concentrations and $^{187}Os/^{188}Os$.

2.2. Apollo 16 impact melt rocks

The Apollo 16 landing site is located within the cratered ancient highlands. At this landing site, two major geologic units were sampled: the Cayley Plains Formation and the Descartes Formation (Fig. 1b; Muehlberger et al., 1980). The Cayley Plains Formation has commonly been interpreted to represent ejecta deposits from the Imbrium basin (Eggleton and Schaber, 1972; Hodges et al., 1973; Ulrich, 1973). Underlying the Cayley Plains Formation, the Descartes Formation has been interpreted to be either deposits of a distinct facies of Imbrium ejecta (Hodges et al., 1973; Ulrich, 1973; Hodges and Muehlberger, 1981), or older ejecta from the Nectaris basin (Wilhelms, 1972; Head, 1974; Stöffler et al., 1981, 1985; Stöffler and Ryder, 2001). Based on age and geochemical constraints, however, Norman et al. (2010) concluded that the contribution of material from the Nectaris basin to the Descartes Formation sampled by Apollo 16 melt rocks was minor.

Since the 1970's, Apollo 16 impact melt rocks have been classified using different chemical criteria. Considerable effort has been focused on classifications based primarily on lithophile element concentrations, but that also utilize concentration data for a limited number of siderophile elements. Most notably, Korotev (1994), following McKinley et al. (1984), divided Apollo 16 melt rocks into four major compositional groups (Groups 1, 2, 3 and 4), as well as several subgroups. Groups 1 and 2 are characterized by higher Sm/Sc ratios than those of Groups 3 and 4. Moreover, in line with the lithophile element concentration, there is a gradual decrease of Sm concentration from Group 1 to 4. In general, Group 1 and 2 melt rocks are relatively mafic, rich in KREEP components and siderophile elements,

while Groups 3 and 4 melt rocks are feldspathic, and comparatively poor in incompatible lithophile and siderophile elements.

By contrast, Fischer-Gödde and Becker (2012) utilized the concentrations of eight HSE, as well as $^{187}Os/^{188}Os$ ratios, to discriminate among the origins of four impact-related rocks from the Apollo 16 site (samples 60315, 67915, 67935, 67955). They reported that these rocks appear to document multiple impactor components with diverse HSE characteristics, varying from chondrite-like to iron meteorite-like.

2.2.1. Regolith breccia 60016—Sample 60016 is a regolith breccia collected near the Lunar Module landing site, located within the Cayley Plains Formation (Ryder and Norman, 1980; McKay et al., 1986; Fig. 1b). This regolith breccia was consolidated at ~3.74 Ga during a basin-forming epoch (Joy et al., 2011), and is composed of both light and dark mineral and lithic clasts, within a finer-grained grey matrix. The clasts include cataclastic and recrystallized anorthosite, poikilitic impact melt rocks, granoblastic material, dark matrix breccias, as well as glass fragments (Ryder and Norman, 1980). Recent petrological, geochemical and geochronological analyses of six, cm-sized clasts extracted from 60016 (Niihara and Kring, 2012a; Swindle et al., 2012; Niihara et al., 2013) showed that these clasts have distinct textures and chemical compositions, consistent with variable amounts of relict minerals (15 to 47%), including olivine, pyroxene and plagioclase, as well as minor opaque minerals (e.g., Fe-Ni metal and troilite). The 60016 clasts are characterized by relatively high K_2O (0.3-0.5 wt.%) and P_2O_5 (0.4-0.5 wt.%) contents, consistent with a KREEP-rich signature, and fall into the Group 1 impact melt rocks defined by Korotev (1994). Similar results for other 60016 clasts are also reported in Korotev (1996). The 60016 clasts are also characterized by variable ^{40}Ar-^{39}Ar plateau ages ranging from 3.7 to 4.0 Ga (Swindle et al., 2012; Niihara et al., 2013). Thus, these lithic clasts were probably generated by several, distinct impact events that either reset or formed the clasts over a several hundred million year period.

Of these six investigated clasts from 60016, we were allocated splits of two: 60016,286b (~0.30 g) and 60016,290b (~0.29 g), where the “b” designation denotes a second fraction of the primary sample (clast), designated “a”, on which the ^{40}Ar-^{39}Ar isotope measurements were made. The three sub-splits of each of the two clasts, ,286a and ,290a, yielded average ^{40}Ar-^{39}Ar plateau ages of 3.878 ± 0.014 Ga and 3.969 ± 0.012 Ga, respectively (Swindle et al., 2012; Niihara et al., 2013).

A prior analysis of a glassy, mafic clast from 60016 gave an Ir concentration of 2.1 ng/g (Korotev, 1996). For this study, HSE concentrations and Os isotopic compositions of 7 and 8 subsamples of clasts ,286b and ,290b, respectively, were determined. In addition, two metal grains extracted from ,290b were processed separately and analyzed.

2.2.2. Impact melt rock 60235—Sample 60235 was collected near the Lunar Module within the Cayley Plains Formation (Fig. 1b). This sample has been described by Ryder and Norman (1980) as a plagioclase-rich basaltic melt rock with a few micrometeorite pits on all sides. It consists of plagioclase laths 200-300 μm long, and interstitial minerals are mainly pyroxene with some mesostasis glass and opaque minerals (Ryder and Norman, 1980).

Lithic clasts consist of plagioclases and plagioclase-rich breccias (Ryder and Norman, 1980). No major/trace element data or age data have been previously reported for this rock. This rock was not classified by Korotev (1994) or subsequent studies. We were allocated ~2.1g of split 60235,11. Consistent with the report of Hunter and Taylor (1981) that there was abundant rust on metal grains in thin sections of 60235, we found that this rock contained small rusted metal grains, as well as sulfides. These metals and sulfides were not separated for individual analysis. The rock was subdivided into 10 subsamples for the analyses of HSE concentrations and Os isotopic compositions.

2.2.3. Impact melt rock 60635—Sample 60635 is a rake sample that was also collected near the Lunar Module within the Cayley Plains Formation (Fig. 1b). It is a coherent, basaltic impact melt rock with abundant laths and prisms of plagioclase and smaller grains of plagioclase and pyroxene as interstitial phases (Dowty et al., 1974; Warner et al., 1976); olivine is absent. Vugs and vesicles are abundant (Ryder and Norman, 1980), and minor phases include nearly pure ulvöspinel, Fe-metal, troilite and K-rich mesostasis (Deutsch and Stöffler, 1987). The Fe-metal grains have relatively high Ni (up to 16%) and Co (up to 1.2%) contents, which Dowty et al. (1974) interpreted as indicating that this rock formed as an impact melt with impactor contamination. This sample consists of two lithologically distinct portions, both with basaltic textures, but different grain sizes. These two portions yielded two Rb-Sr ages of 3.93 ± 0.02 and 3.81 ± 0.03 Ga (Deutsch and Stöffler, 1987), recalculated (using a λ for ^{87}Rb of 1.397×10^{-11} yr^{-1} from Rotenberg et al. (2012)), which were interpreted to suggest that the fine-grained fragment with the older age was incorporated into the younger host lithology that Deutsch and Stöffler (1987) classified as a member of the Anorthositic Noritic Melt Rock group. This also means that these two portions of the rock were derived from two separate impact events. We were allocated ~2.0 g of split 60635,18. This rock was coarse-grained, implying that it belonged to a portion of the younger host lithology, which Korotev (1994) classified as a Group 3 melt rock. The allocated sample was extremely friable, and no metal grains were extracted. Ten subsamples were processed for the analyses of HSE concentrations and Os isotopic compositions.

2.2.4. Impact melt rock 62295—Sample 62295 is a coherent basaltic impact melt rock that was collected near Buster Crater within the Cayley Plains Formation (Fig. 1b). It has numerous micrometeorite pits on the “lunar top” side, and none on the opposing side. This sample has been described as a spinel troctolite with an approximate mineralogical mode of 55% plagioclase, 25% olivine, 5% spinel, and 15% mesostasis (Ryder and Norman, 1980). Xenocrysts of Mg-rich olivine (Fo_{90-95}), Ca-rich plagioclase (An_{94-99}), pink spinel (9-16% chromite) and metal grains are found throughout the fine-grained matrix (Ryder and Norman, 1980). Sample 62295 is very Mg rich (MgO = 14.7%) with one of the highest Mg# (molar Mg/(Mg+Fe)x100 = 81) of any lunar impact melt rocks analyzed. It has been classified as a Group 2 melt rock (Korotev, 1994). The rare earth element (REE) concentrations in this rock are high, and the REE pattern for this rock is dominated by a KREEP-rich signature (Hubbard et al., 1973; Wänke et al., 1976). The high contents of siderophile elements (Ni = 215 to 330 μg/g; Ir = 3.6 to 5.5 ng/g; Au = 3.1 to 7.0 ng/g; e.g., Krähenbühl et al., 1973; Wänke et al., 1976), along with the presence of metal grains,

indicate impactor contamination. This sample has been dated via the ^{40}Ar-^{39}Ar method, yielding an age of 3.886 ± 0.012 Ga (Norman et al., 2006).

We were allocated ~2.0 g of split 62295,188. The rock was dark in color and contained macroscopic plagioclase crystals with some large olivine grains up to ~1 mm in diameter. It also contained irregular vugs (up to 1 mm across). No metal grains were observed. This rock was subdivided into 9 subsamples that were processed for HSE concentrations and Os isotopic compositions.

2.2.5. Impact melt rock 63549—Sample 63549 is a rake sample with numerous micrometeorite pits. It is an olivine-free, fine-grained, basaltic melt rock containing plagioclase laths 50-100μm long (Vaniman and Papike, 1981) and zoned pyroxenes (Warner et al., 1973), as well as a glassy mesostasis and opaque minerals. It has no relict minerals or lithic clasts, indicating that it was initially totally molten (Gooley et al., 1973). The rock is highly enriched in Al (Al_2O_3 = 26.5 to 29.8%) compared to other Apollo 16 basaltic impact melt rocks, and is consistent with classification as a Group 3 melt rock. The relatively high contents of siderophile elements (Ir = 7.8 to 9.0 ng/g; Au = 3.1 to 3.6 ng/g; Boyton et al., 1976; Wasson et al., 1977) indicate that it is an impact melt rock with moderate impactor contamination. This is consistent with the presence of metal grains in the sample that have high Ni (14 to 16%) and Co (1.0 to 1.3%) contents (Gooley et al., 1973). Sample 63549 has been dated via the ^{40}Ar-^{39}Ar method to be 3.840 ± 0.011 Ga (Norman et al., 2006). As a consequence of its younger age, it was interpreted to have formed in an event that was distinct from the impact that generated 62295. We were allocated ~1.9 g of split 63549,33. This fragment has two visually distinct regions: one dark and fine-grained, the other light and coarse-grained region. We were unable to separate the two regions for individual chemical analyses. No metal grains were extracted. The rock was subdivided into 9 subsamples for the analysis of HSE concentrations and Os isotopic compositions.

2.2.6. Regolith breccia 65095—Sample 65095 is partially coated by black glass. This sample was collected on the lower slopes of the Stone Mountain, on the boundary between the Cayley Plains Formation and the Descartes Formation (Fig. 1b). It is composed of large clasts of impact melt rock enclosed in a friable matrix. The melt rock clasts contain grains of plagioclase, mafic minerals, and opaque minerals (metal, troilite, ilmenite and spinel), as well as basaltic impact melt rock and cataclastic anorthosite (McKay et al., 1986). Recent petrological and geochemical studies of three enclosed lithic clasts extracted from 65095 (subsamples ,115; ,116; ,118) reported that all three clasts have fine-grained, subophitic textures primarily consisting of pyroxene and plagioclase, as well as minor olivine, ilmenite, armalcolite, Fe-Ni metal and rust (Niihara and Kring, 2012b). These clasts have comparable relict mineral and bulk compositions, suggesting similar origins. The 65095 clasts also have bulk compositions similar to Group 2 melt rocks. Of these three clasts, we were allocated ~ 0.2 g of ,106b, which is a split of clast ,118. The ^{40}Ar-^{39}Ar analysis of three sub-splits of another fraction of this clast ,106a, yielded no plateau age, probably due to subsequent disturbance, but the average age for the best heating steps with highest ages was 3.884 ± 0.017 Ga (Niihara et al., 2013).

Previous studies of the chemical composition of 65095 revealed that all the splits from this breccia have relatively high Ir (1.7 to 11.8 ng/g) and Au (2.8 to 7.5 ng/g) concentrations, evidence of impactor contamination (Krähenbühl et al., 1973; McKay et al., 1986; Korotev, 1996). To further explore the origins of the HSE in this complex rock, 8 subsamples of clast ,106b were processed for HSE concentrations and Os isotopic compositions.

2.2.7. Impact melt rock 67095—Sample 67095 is a basaltic impact melt rock that was collected from the rim of the North Ray Crater (Fig. 1b). Formation of this crater has been inferred to have excavated materials from the underlying Descartes Formation (Stöffler et al., 2006). According to Warren and Wasson (1978), this rock is composed of plagioclase (62%), pyroxene (17%) and olivine (12%). The bulk composition of the rock reveals that 67095 is significantly more mafic than other impact melt rocks and soils from the same locale, and is a member of Group 2 melt rocks (McKay et al., 1981; Fagan et al., 2013). Prior studies of the chemical compositions of the interior of 67095 have noted impactor contamination, evinced by relatively high Ir (1.4 to 5.8 ng/g) and Au (1.2 to 6.8 ng/g) concentrations in all the melt splits (e.g., Warren and Wasson, 1978; Lindstrom and Salpus, 1981). The ^{40}Ar-^{39}Ar analysis of three sub-splits of subsample 67095,124 yielded a minimum formation age of 3.878 ± 0.022 Ga, with a thermal disturbance as recently as 1.3 Ga (Fagan et al., 2013).

We were allocated ~2 g of split 67095,125, immediately adjacent to ,124. The rock was very friable and easily broken into smaller pieces using ceramic tweezers. The sample processed contained substantial Fe-Ni metal and troilite. Sizable (~100-350 μm) metal grains were separated for laser ablation-ICP-MS analysis, and some were subsequently individually digested for the measurement of HSE concentrations and Os isotopic compositions. The remaining bulk rock was subdivided into 10 subsamples that were also dissolved and analyzed for HSE concentrations and Os isotopic compositions.

2.2.8. Impact melt rock 68416—Sample 68416, and the petrologically similar sample 68415 that was collected nearby, have been described as recrystallized impact melt rocks (Ryder and Norman, 1980). Both rocks were chipped from the top of a 0.5m boulder on the rim of a 5 m crater within a ray from the South Ray Crater, within the Cayley Plains Formation (Fig. 1b). They have igneous, intersertal textures characterized by “fretworks” of plagioclase (73-82%) laths with interstitial olivine (2-7%) and pyroxene (12-20%), as well as minor opaques (dominant ilmenite up to 2%, with some Fe-Ni metal and troilite), phosphates, residual glass and other minerals (*Lunar Sample Compendium*). They are classified as Group 3 melt rocks. Both 68416 and 68415 have been dated at 3.82 ± 0.01 Ga using the internal Rb-Sr isochron technique (Papanastassiou and Wasserburg, 1972; Reimold et al., 1985), and recalculated using a λ for ^{87}Rb of 1.397x10^{-11} yr^{-1} (Rotenberg et al., 2012). This age is within the range of ages for aluminous subophitic Apollo 16 impact melt rocks (Norman et al., 2006). An older ^{40}Ar-^{39}Ar age of 4.1 Ga for a plagioclase separate may be due to contamination of some plagioclase xenocrysts (Huenke et al. 1973). Previously reported HSE concentrations for 68415 were relatively high (Ir = 4.6-11.8 ng/g, and Au = 2.0-8.3 ng/g), indicating substantial impactor contamination, and consequently, an impact origin (Krähenbühl et al., 1973; Wasson et al., 1975). We were allocated an ~2.0 g

split of 68416,16 which was coherent and dense. Ten subsamples were processed for HSE concentrations and Os isotopic compositions.

3. ANALYTICAL METHODS

All samples were initially examined, photographed and visually characterized using a binocular microscope. Each rock (0.2-2 g) was then gently broken up using an alumina mortar and pestle, and divided into approximately ten subsamples weighing between 10 and 200 mg each. Subsamples were gently further de-comminuted using the mortar and pestle, but not finely ground, in order to avoid smearing of metal. For some samples, sizable metal grains were separated from silicate fractions. Each separated metal grain (laser ablation ICP-MS analyses were performed for some metals before dissolution; see details below) or subsample of bulk rock, was weighed and sealed in pre-cleaned Pyrex Carius tubes, with appropriate amounts of mixed ^{185}Re-^{190}Os and ^{191}Ir-^{99}Ru-^{194}Pt-^{105}Pd spikes, 3 ml of conc. HNO_3, and 2 ml of conc. HCl. Samples were digested at 270ºC for >72 hours. Osmium was extracted immediately from the acid solution after digestion by solvent extraction into CCl_4, then back extracted into HBr (Cohen and Waters, 1996). The Os fraction was purified via microdistillation from a H_2SO_4-dichromate solution into 15μl of HBr (Birck et al., 1997). Iridium, Ru, Pt, Pd and Re were separated and purified from the remaining acid solution via anion exchange column chromatography (Rehkämper and Halliday, 1997).

Osmium isotope compositions were determined as OsO_3^- using an electron multiplier on a thermal ionization mass spectrometer (*Thermo Fisher Triton*) in a peak-hopping mode at the University of Maryland (UMd). In order to enhance oxide production, an O_2 bleed valve was used to establish a pressure of ~$8x10^{-8}$ mbar in the mass spectrometer source chamber. Oxygen correction was accomplished using $^{17}O/^{16}O = 0.0003749$ and $^{18}O/^{16}O = 0.0020439$, followed by instrumental mass fractionation correction using $^{192}Os/^{188}Os = 3.08271$. The potential ^{187}Re isobaric interference on ^{187}Os was monitored by measuring mass 233 ($^{185}ReO_3^-$), which was generally less than 2 counts per second (cps). No corrections were made for this. The internal precisions for all $^{187}Os/^{188}Os$ measurements were better than ±0.1%. The external precision for $^{187}Os/^{188}Os$ ratios of 350-500 pg loads of the Johnson-Matthey Os UMd reference solution during the period of data collection (September 2011 to December 2013) averaged at 0.11374 ± 21 ($2\sigma_{stdev}$, n = 39). The reported $^{187}Os/^{188}Os$ ratios of samples were corrected for instrumental bias, typically less than 0.1%, using the correction factor, which was calculated by dividing the recommended value of 0.113787 measured on the Faraday cups of the UMd Triton (Walker, 2012) by the average measured $^{187}Os/^{188}Os$ of the standard in each analytical session.

All HSE column cuts were dissolved in 5% HNO_3 and measured using either the triple electron multipliers of a *Nu Plasma* inductively coupled plasma mass spectrometry (ICP-MS) or using a single electron multiplier collector of an *Element 2* ICP-MS at UMd. Instrumental mass fractionation was corrected by periodic measurements of in-house standards (usually one per three samples analyzed) using the standard-bracketing method. For the Pd analysis using the *Nu Plasma*, zirconium (^{90}Zr) was monitored to qualitatively judge the isobaric interference of $^{90}ZrO^+$ on mass 106; the signal of ^{90}Zr was usually less than a few mV, and the isobaric interference of $^{90}ZrO^+$ on mass 106 was negligible. For

the Pd analysis using *Element 2*, yttrium (^{89}Y) and zirconium (^{90}Zr) standard solutions were measured to determine the oxide production rate (MO^+/M^+), which was generally less than 0.2%. Given very low signals (less than 2000 cps) of $^{89}Y^+$ in the sample solutions, the calculated signals of $^{89}YO^+$ were negligible for isobaric interference on mass 105; by contrast, the isobaric interference correction of $^{90}ZrO^+$ on mass 106 was 0.03-2.1% (variably depending upon the Zr/Pd ratios in the sample solutions) with an average of ~0.6%. Diluted, spiked solutions of the iron meteorites South Byron (for Ir and Pt), Dronino (for Re), and Sikhote-Alin (for Ru) were run during each analytical session as secondary standards; no Pd meteoritic aliquots were run. The isotopic ratio results of these runs were within 2% with those accredited values obtained from precise measurements of undiluted sample solutions using Faraday cups of the *Nu Plasma.*

Total analytical blanks measured during the period of lunar sample analyses yielded an average $^{187}Os/^{188}Os$ of 0.163 ± 0.013, and 0.13 ± 0.06 pg Os, 0.43 ± 0.17 pg Ir, 3.4 ± 1.6 pg Ru, 4.2 ± 1.5 pg Pt, 3.5 ± 3.2 pg Pd, and 0.9 ± 0.6 pg Re (1σ, n = 10). All reported HSE concentrations and Os isotopic data were corrected for blank contributions. The blank contributions for the lunar samples were: Os 0.01-0.3%, Ir 0.03-0.6%, Ru 0.09-1.9%, Pt 0.09-1.6%, Pd 0.08-1.7%, and Re 0.5-14%. The precision of the reported HSE concentrations of the lunar samples estimated from the blank contribution, variation in the blank and uncertainties on the measured isotopic ratios was on average better than 0.5% for Os, 2% for Ir, Ru, Pt and Pd, and 5% for Re, unless stated otherwise in the tables and/or text. Because the acid digestion procedure used did not include hydrofluoric acid (digestions were accomplished in borosilicate vessels), silicates were not completely dissolved by the process, but the retention of HSE in residual silicates was negligible as discussed in the Electronic Annex.

For the melt rock 67095, sizable separated metal grains (see images in Fig. EA1 in the Electronic Annex) were attached to a glass slide using double-sided tape before dissolution for bulk analyses of HSE concentrations and Os isotopic compositions described above. The *in situ* surface to interior materials of sample grains were ablated and analyzed using a *New Wave Research* UP-213 laser-ablation system coupled to a *Thermo-Finnigan* ICP-MS (*Element 2*) at the University of Maryland. Ablated material was transported from the ablation cell by a 1 L/min He gas flow, mixed with a 0.6 L/min Ar gas flow, and then introduced to the ICP torch. The ablation spot sizes ranged from 55 to 80 μm, the laser power was controlled to be between 2.0 and 2.3 Jcm^{-2}, and the repetition pulse rate was 7 Hz. Isotope masses were measured for 5 ms per cycle with 180 cycles per analysis. No ablation occurred in the first 20 seconds of each analysis for background count determination. The system was flushed with He for 2 minutes between analyses. Isotopes monitored and reported here (averages for more than one isotope) were: ^{57}Fe, ^{59}Co, ^{61}Ni, ^{62}Ni, ^{66}Zn, ^{67}Zn, ^{69}Ga, ^{73}Ge, ^{99}Ru, ^{101}Ru, ^{103}Rh, ^{105}Pd, ^{106}Pd, ^{185}Re, ^{189}Os, ^{192}Os, ^{193}Ir, ^{194}Pt, ^{195}Pt, and ^{197}Au. Data reduction was performed using *Lamtrace* (Achterbergh et al., 2001) assuming an Fe concentration of 90% for all metals as the internal standard, with iron meteorites Hoba, Filomena and Coahuila utilized as reference materials for Co, Ni, Zn, Ru, Rh, Pd, Re, Os, Ir, Pt and Au (average results reported from the three standards), and Hoba for Ga and Ge. Concentrations were finally normalized based on an inferred Fe concentration that yielded a sum of Fe+Ni+Co of 100%. The detection limits were

determined using the background count rate plus three times the standard deviation of the background.

4. RESULTS

4.1. Bulk HSE concentrations and Os isotopic compositions of impact rocks and metals

Bulk HSE concentrations and Os isotopic compositions were determined by isotope dilution for a total of 110 subsamples (including both silicate fractions and individual metal grains) of the eleven rocks examined here. These data are provided in Table 2.

4.1.1. Re-Os isotope systematics—The ^{187}Re–^{187}Os isotope system is based on the beta decay of ^{187}Re to ^{187}Os, with a $\lambda = 1.666 \times 10^{-11}$ yr^{-1} (Smoliar et al., 1996). For the purposes of this study, Os isotopic compositions were primarily treated as a proxy for the time-integrated Re/Os of the materials analyzed, but isotopic systematics with respect to age information was also considered. Because $^{187}Os/^{188}Os$ can be precisely measured, this ratio provides a robust constraint on the long-term Re/Os of a sample (e.g., Puchtel et al., 2008; Fischer-Gödde and Becker, 2012; Sharp et al., 2014). Thus, in addition to direct measurement of Re, concentrations of Re can be calculated (Re*) based upon measured Os concentrations and Os isotopic compositions, assuming that the Re/Os of each subsample was established from an early solar system reservoir with an initial $^{187}Os/^{188}Os$ of 0.09516 at 4.568 Ga (Smoliar et al., 1996). For most samples analyzed here, calculated and measured Re concentrations are indistinguishable within uncertainties (≤ ±5%), indicating that the Re-Os isotope systematics, and presumably the systematics of other HSE, remained essentially closed, subsequent to formation. The major exception to this is sample 60235, which is characterized by several subsamples with measured Re concentrations that are considerably higher (>10%) than Re*.

The average $^{187}Os/^{188}Os$ ratios of subsamples of the Apollo 15 impact melt rocks 15445 and 15455 are 0.1348 ± 0.0007 ($2\sigma_{mean}$, n = 10) and 0.1372 ± 0.0004 (n = 11), respectively. These ratios are higher than most bulk chondrites, which range mainly from 0.125 to 0.133 (Chen et al., 1998; Walker et al., 2002; Brandon et al., 2005a,b; Fischer-Gödde et al., 2010; van Acken et al, 2011).

Apollo 16 impact melt rocks 60235, 62295 and 67095 are characterized by broadly similar average $^{187}Os/^{188}Os$ ratios of 0.1362 ± 0.0010 (n = 10), 0.1343 ± 0.0010 (n = 9), and 0.1356 ± 0.0010 (n = 15; including 10 silicate fractions and 5 metal grains), respectively. By contrast, subsamples of the impact melt rocks 60635, 63549 and 68416, are characterized by considerably lower average $^{187}Os/^{188}Os$ ratios of 0.1297 ± 0.0009 (n = 10), 0.1300 ± 0.0009 (n = 9), and 0.1297 ± 0.0006 (n = 10), respectively. The isotopic data for all three of these samples are within the range of bulk chondrites.

The clasts extracted from the Apollo 16 regolith breccias are characterized by higher $^{187}Os/^{188}Os$ ratios. Subsamples of clasts 60016,286b, 60016,290b and 65095 have $^{187}Os/^{188}Os$, averaging 0.1383 ± 0.0010 (n = 7), 0.1390 ± 0.0008 (n = 11; including 9 silicate fractions and 2 metal grains), and 0.1392 ± 0.0020 (n = 10), respectively. Individual metal grains from 60016,290b and 67095,125 are characterized by two to three orders of magnitude

higher Re and Os concentrations (and other HSE; see below), compared to their host rocks, but essentially identical $^{187}Os/^{188}Os$ to the host rock. These ratios are also comparable to averages for Apollo 16 poikilitic impact melt rock 60315, and subophitic impact melt rock 67935, for which Fischer-Gödde and Becker (2012) reported $^{187}Os/^{188}Os$ ratios of 0.1398 ± 0.0007 (n = 10) and 0.1362 ± 0.0027 (n = 10), respectively.

Fischer-Gödde and Becker (2012) reported a Re-Os isochron age of 4.21 ± 0.13 Ga for subsamples of Apollo 16 impact melt rock 67935. To assess whether data for any of the eleven samples examined here form linear trends that could be interpreted as isochrons, data for subsamples are plotted on $^{187}Re/^{188}Os$ versus $^{187}Os/^{188}Os$ diagrams (Fig. 2). There are no obvious, well-defined trends for any of the rocks, but some aspects of these plots will be discussed below.

4.1.2. HSE concentrations and ratios—Subsamples of most of the lunar impact melt rocks examined here are characterized by more than twofold variations in HSE concentrations (Table 2). This level of variation is common for subsamples of impact melt rocks from other Apollo sites (e.g., Norman et al., 2002; Puchtel et al., 2008; Sharp et al., 2014). Of note, the mass-weighted average HSE concentrations of clasts extracted from the regolith breccias are significantly higher than those of the bulk impact melt rocks. For example, the average Ir concentrations of clasts 60016,286b and ,290b are 13.7 and 24.6 ng/g, respectively, compared to the average concentration of 3.4 ng/g for 67095. The average Ir concentration of clast 65095 is similarly high at 24.5 ng/g. Of the metal grains extracted from 60016,290b and 67095, their bulk HSE concentrations are two to three orders of magnitude higher than the host rocks (Table 2), but their relative HSE concentrations are similar to the host rocks. The CI chondrite-normalized HSE patterns for bulk rocks and metal grains are provided in Fig. EA2 in the Electronic Annex.

Impact-generated terrestrial rocks commonly show linear trends between Ir and other HSE as a result of variable contamination by HSE-rich meteoritic materials (Koeberl, 1998; MacDonald et al., 2001). Where the concentrations of HSE in target rocks are very low, the calculated slopes of regression trends of HSE versus Ir can be used to constrain the relative concentrations of the HSE that characterized the impactor, and the y-axis intercepts of the trends provide constraints on the HSE budget of the target rocks (e.g., McDonald et al., 2001). The same approach is taken here for lunar impact melt rocks.

For different subsamples of each of the lunar impact rocks examined here, Ir concentrations are generally well correlated with the concentrations of other HSE (Fig. 3), consistent with observations presented in prior studies of lunar impact melt rocks (Puchtel et al., 2008; Fischer-Gödde and Becker, 2012; Sharp et al., 2014). For each sample, slope derived HSE/Ir ratios, along with the intercepts and statistical uncertainties, were determined by linear regression of HSE versus Ir concentrations using the ISOPLOT least squares regression program (Ludwig, 2003) (Fig. 3). Analytical uncertainties (2σ) for the concentration data used for the regression calculations were conservatively set as 0.2% for $^{187}Os/^{188}Os$, 0.5% for Os, 2% for Ir, Ru, Pt and Pd, and 5% for Re. For 67095, silicate fractions and metal grains were both separately and collectively regressed. Regression results are summarized in Table 3.

For samples 60016,286b, 60016,290b, 60235 and 65095, the Ru/Ir, Pt/Ir and Pd/Ir regressions are characterized by scatter that is greater than can be accounted for by analytical uncertainties, as well as non-zero y-intercepts. Possible reasons for the scatter will be discussed below. The averages of the HSE/Ir ratios of all of the combined subsamples of each of these rocks are also provided in Table 3.

4.2. *In situ* siderophile element concentrations of 67095 metals

Six metal grains extracted from sample 67095,125 were analyzed for siderophile element (including HSE) concentrations using laser ablation ICP-MS (Table 4). All but one of the grains had sufficiently high concentrations of siderophile elements for precise measurement. Grain M11 had siderophile element concentrations near or below detection limits.

Initial laser ablation of grains M1 and M6 accessed the rims of these metals. Continued ablation accessed the inner portions of each grain, here termed cores (see time-resolved intensity spectra in Fig. EA3 of the Electronic Annex). The grain cores are characterized by broadly chondritic relative concentrations of siderophile elements (Fig. 4). In contrast to the cores, the grain rims are characterized by significantly lower Re, Os, Ir, Pt, slightly higher Ru and Pd, and significantly higher Ni concentrations (Fig. EA4). Both rims and cores are strongly depleted in volatile siderophile elements (Zn, Ga, and Ge). Generally similar compositions were reported for the rims of metal grains from Apollo 17 melt rock 76215 (James et al., 2007) and the cores of metal grains from Apollo 16 melt rock 67955 (Norman and Nemchin, 2014). Grains M3, M9, and M10 were so small that signal was integrated over the complete analysis of each grain. Grains M3 and M10 are compositionally similar to the rims of the larger grains, whereas the composition of grain M9 is more similar to the compositions of the cores of the larger grains. In addition, the HSE concentrations of bulk grains M1 and M6 are intermediate between the concentrations in their respective rims and cores.

5. DISCUSSION

5.1. Origin of Apollo 16 metals

Metals contained in lunar impact melt rocks can originate in multiple ways. They may be endogenous lunar metal derived from target crustal rocks, or exogenous metal from either an earlier impactor or the impactor that created the melt rocks. In any case, the metal can partially or wholly equilibrate with melt or vapor during the impact, so neither endogenous nor exogenous metal necessarily provides an unassailable chemical signature of the ultimate source of the metal (Axon and Goldstein, 1973; Misra and Taylor, 1975). Metal may also directly condense from a vapor phase into vesicles at the time of formation of the impact melt rock. The latter type of metal typically occurs as well-formed crystals, and can similarly include chemical components from both exogenous and endogenous sources (Misra and Taylor, 1975).

Because of the lack of well-formed crystals, the metal grains studied here likely represent the trapping of endogenous or exogenous molten metal in the cooling melt sheet. Of these grains, the laser ablation ICP-MS data reveal that metal grain M11 is characterized by

the lowest, and most fractionated HSE concentrations of the grains analyzed (Table 4; Fig. 4). This could indicate that the grain represents evolved metal that formed by solid metal-liquid metal fractionation in the impactor. Based on the studies of magmatic iron meteorites (Wasson, 1999; Wasson and Richardson, 2001; Campbell and Humayun, 2005; Wasson et al., 2007; Walker et al., 2008; McCoy et al., 2011), however, highly fractionated metal formed in this manner might also be expected to have developed higher Ni and Co concentrations than less evolved metals (Fig. EA5). This grain has similar or lower Ni and Co concentrations compared to the HSE-rich grains that are presumed to derive from the impactor, as discussed below. More likely, the low and fractionated HSE concentrations of this grain suggest that it is endogenous, HSE-poor metal with little exogenous HSE (Misra and Taylor, 1975). This grain contains relatively high concentrations of Au, and to a lesser extent Pd. These are the two HSE with the lowest 50% condensation temperatures and, along with Re, are normally the only HSE that behave incompatibly in silicate systems (Pearson et al., 2004). Thus, the HSE concentrations in this grain may reflect characteristics of lunar crustal target rocks, or incorporation of Au and Pd resulting from volatility effects.

The other metal grains from sample 67095, and the two grains from 60016,290b are comparatively rich in HSE, consistent with derivation of the HSE, and possibly the metal itself, from a meteoritic impactor. For the 67095 grains, the limited variations in bulk HSE concentrations, and the well-defined linear correlations between Ir and other HSE (Fig. 3), suggest that these metals formed concurrently from a single impactor. The bulk metal grains and the bulk silicate subsamples have similar chondrite-normalized HSE patterns (Fig. 4; Fig. EA2), and their slope derived HSE/Ir ratios and $^{187}Os/^{188}Os$ are identical within uncertainties (Table 3). The bulk grain HSE patterns and $^{187}Os/^{188}Os$ for 60016,290b are also similar to their associated bulk silicate subsamples (Fig. EA2). In neither case is this surprising, as the siderophile elements present in the bulk subsamples of these rocks mostly are sited in metal grains (see below).

Although the ranges of $^{187}Os/^{188}Os$ ratios of grains from the two samples overlap, the 60016,290b grains are, on average, ~2% higher. If all grains examined were derived from the same impactor, the variability requires modest modification of Re/Os by either crystal-liquid fractionation processes, or equilibration with surrounding vapor or melt. Indeed, the effects of crystal-liquid fractionation, metal-silicate or metal-vapor equilibration are observed in the rim versus core concentrations of siderophile elements for the 67095 grains. Nickel contents in the cores (2.8 to 4.9 wt.%) are substantially lower than in rims (9.9 to 14.9 wt.%) (Table 4; Fig. EA4). Further, the rims are depleted in Co, Ga, Ge, Re, Os, Ir, Pt and Au, compared to the cores, whereas Ru and Pd are enriched (Fig. EA4). Rhodium is the only siderophile element that shows little difference in concentration between rim and core.

The cause of the fractionation of siderophile elements between the rims and cores of these metal grains remains elusive. Some of the element variations are consistent with the general effects of solid metal-liquid metal fractionation, as observed in magmatic iron meteorite groups (e.g., Pernicka and Wasson, 1987). For example, elements such as Re, Os and Ir normally behave compatibly with solid metal, whereas Pd normally behaves incompatibly. Hence, the concentration variations of these elements are broadly consistent with outward crystallization of the metal grains. However, it is difficult to envision how these small metal

grains could have slowly crystallized from their centers to rims. Further, Ru is significantly enriched, and Au significantly depleted, in the rims, compared to the cores, and this runs counter to the behavior of these two elements in magmatic iron systems. Thus, fractional crystallization of the metal does not appear to be a viable explanation for the elemental concentration differences between cores and rims.

It is also possible, that diffusion or equilibration between the rim and surrounding vapor or silicate melt could have resulted in the observed compositional differences. However, this option too seems improbable, given the highly siderophile natures of elements such as Os and Ir, yet lower concentrations in the rims.

Instead, we speculate that the most likely cause for the distinct rim compositions is that they represent metal formed as condensate upon metal derived from the impactor. Thus, the concentrations of the siderophile elements present in the rims may reflect both the composition of the direct condensate, coupled with some degree of post-condensation diffusive equilibration between the core and rim.

5.2. Osmium isotope and HSE compositions

5.2.1. Comparison of HSE concentrations—Consistent with prior studies (Korotev et al., 2003; James et al., 2007; Fischer-Gödde and Becker, 2012; Sharp et al., 2014; Norman and Nemchin, 2014), the metal grains extracted from impact melt rock 67095 and clast 60016,290b are characterized by two or three orders of magnitude higher HSE concentrations, compared to their host rocks (Table 2). Assuming all HSE in the bulk impact melt rocks were sited in metals, using the average composition of the 67095 metal grains for all the impact melt rocks (Table 2, excluding grain M3 that had a significant portion of silicate lowering the concentrations), mass balance calculations indicate that ~0.2 wt.% of metal would be required to account for the average HSE composition of sample 67095, and 0.2 to 0.8 wt.% for those of the other impact melt rocks.

Mass balance calculations for lithic clast 60016,290b, using the average concentrations for the metal and bulk fractions, suggest that 2.5 wt.% of metal would be required to account for its average bulk HSE composition, and 1.3 to 2.5 wt.% for those of the other lithic clasts. These projected abundances of metal are similar to estimates derived from Ni concentrations in the metals relative to bulk samples for Apollo 16 Group 1 and 2 melt rocks (Korotev, 1994, 2000). The higher proportion of metal in the lithic clasts can potentially explain why the average HSE concentrations of lithic clasts extracted from the regolith breccias (60016 and 65095), are significantly higher than the concentrations in the bulk impact melt rocks examined here (15445, 15455, 60235, 60635, 62295, 63549, 67095 and 68416) and from other studies (Norman et al., 2002; Puchtel et al., 2008; Fischer-Gödde and Becker, 2012; Sharp et al., 2014). To account for the difference in proportion of metal, we suggest that the lithic clasts may have accumulated metal from multiple impactors over a substantial period of time before consolidation into the regolith breccias. Accumulation of diverse metal has led to higher siderophile element concentrations, and as discussed in the next section, considerable dispersion about the HSE trends.

5.2.2. Causes for scatter and non-zero y-intercepts on Ir-HSE mixing plots—

If a lunar impact melt rock consists of a simple two-component mixture of a HSE-rich impactor component and the essentially HSE-free pristine lunar crust, regressions of one HSE versus another from subsamples of the rock should yield linear trends with y-intercepts of zero, and the slopes of these trends can be used to approach the elemental ratios of the impactor component (Puchtel et al., 2008). Data for subsamples of six of the Apollo 15 and 16 samples examined here (15445, 15455, 60635, 62295, 67095, 68416) are characterized by forming well-defined linear correlations of HSE versus Ir, with y-intercepts that are statistically indistinguishable from zero (Fig. 3; Table 3). Consequently, these impact melt rocks are interpreted to be dominantly two-component mixtures with the HSE revealing the chemical signature of the impactor that generated the rocks.

Linear regression results for impact melt rock 63549 are statistically poorer than for the aforementioned samples, yet the trends for all HSE show near-zero y-intercepts. The larger uncertainties in both the regressions and intercepts primarily stem from the very limited variations in HSE concentrations. For example, Ir ranges only from 8.1 to 12.4 ng/g (Table 2). Thus, the HSE systematics of this sample are considered to be well behaved and consistent with simple two-component mixing. This is also consistent with the observation that no relict minerals or lithic clasts are present in the rock (Gooley et al., 1973).

By contrast, the correlations of HSE versus Ir for subsamples of impact melt rock 60235, as well as the two lithic clasts from sample 60016, and the single lithic clast from 65095 are characterized by greater scatter and/or non-zero y-intercepts for Ru, Pt and Pd (Fig. 3; Table 3). Similar levels of scatter and non-zero y-intercepts have been reported for other Apollo 16 and 17 lunar impact melt rocks (Puchtel et al., 2008; Fischer-Gödde and Becker, 2012; Sharp et al., 2014).

Because scatter and/or non-zero y-intercepts may hamper characterizing the chemical composition of the impactors, it is important to investigate the possible causes. For the scatter observed in some Apollo 16 and 17 impact melt rocks, Fischer-Gödde and Becker (2012) and Sharp et al. (2014) systematically considered four possible causes: post-formation open-system behavior, analytical artifacts, fractionation of HSE within the melt sheet by volatilization or crystallization, and incorporation of HSE from multiple impactors. Because we used similar analytical methods and observe similar deviations from linear trends, we follow the arguments presented by Puchtel et al. (2008), Fischer-Gödde and Becker (2012), Sharp et al. (2014), and do not further consider the possibilities that analytical artifacts or late-stage open-system behavior were primary factors in generating the scatter and non-zero y-intercepts. Fractionation of HSE in the evolving melt sheet and incorporation of materials from diverse impactors, however, remain viable candidates for generating the scatter.

The three lithic clasts extracted from regolith breccias 60016 and 65095 show considerable scatter in trends defined by Ru, Pt and Pd versus Ir, as well as positive y-intercepts for these trends (Fig. 3). These characteristics could reflect the fractionation of HSE within the melt sheet at the time of impact, resulting from large-scale volatilization and crystal-liquid fractionation. These effects could mimic the small scale effects observed in the core versus

rim heterogeneities present in metal grains discussed above. Consequently, one possible means of generating scatter within an individual sample would be through incorporation of metal grains formed in different parts of the chemically evolving melt sheet.

Although this possibility cannot be ruled out for all samples characterized by poorly defined HSE trends, there is some evidence that this process does not account for the scatter in clast 65095,106b. Data for eight subsamples of the clast define a relatively precise $^{187}Re/^{188}Os$ versus $^{187}Os/^{188}Os$ trend that defines an apparent Re-Os isochron age of 1.98 ± 0.57 Ga (MSWD = 8.5). This age is considerably younger than the ^{40}Ar-^{39}Ar formation age of ~3.88 Ga determined for the spatially associated fraction ,106a (Swindle et al., 2012; Niihara et al., 2013). Given the good positive correlation between $^{187}Os/^{188}Os$ and 1/Os of the subsamples (Fig. 2j), the Re-Os correlation is best interpreted as a mixing line between two Re- and Os-rich components with different $^{187}Os/^{188}Os$ ratios at the time of formation, rather than a closure age. Chemical evolution in a melt sheet can likely cause changes in elemental ratios, but cannot affect radiogenic isotopic compositions. Consequently this sample requires a different explanation for the scatter and non-zero intercepts of its HSE data.

A more parsimonious explanation for the scatter and non-zero intercepts of the lithic clasts is that they incorporated metal grains derived from two or more impactors that had different HSE characteristics. This is consistent with the observation that these clasts have higher concentrations of HSE, resulting from the presence of more metal, compared to the impact melt rocks (see above), and is also consistent with the Re-Os isotopic systematics of 65095,106b.

Assuming that there were two impactor components that were variably incorporated within the lithic clasts, three-component mixing would lead to the creation of fields on plots of HSE versus Ir, rather than linear trends. Of the three Apollo 16 lithic clasts, subsamples are all characterized by higher Ru/Ir, Pt/Ir, Pd/Ir and $^{187}Os/^{188}Os$ ratios than bulk chondrites, suggesting that an impactor component that is termed here as “X”, was characterized by suprachondritic ratios involving these elements, while the second impactor component, termed here as “Y”, is assumed to be characterized by less suprachondritic or chondritic ratios. The schematic relationship of impactors X and Y in HSE versus Ir plots is illustrated in Fig. 5a. If X, compared to Y, imparts the greater proportion of HSE into the impact melt, of which the HSE composition approaches the X composition, this would lead to the creation of HSE versus Ir trends with scatter primarily controlled by the variable HSE contribution from Y, as well as negative y-intercepts (Fig. 5b). This is inconsistent with the prevailing positive y-intercepts of the lithic clasts. On the other hand, if Y is the dominant impactor imparting the greater proportion of HSE, this would cause HSE versus Ir trends with scatter and positive y-intercepts (Fig. 5c). This scenario can account for the characteristics of the data for the lithic clasts. The fact that Re and Os y-intercepts in the regression trends of these lithic clasts are typically indistinguishable from zero within uncertainties (Table 3; Fig. 3) is primarily due to relatively limited inter-elemental variations of Re, Os and Ir among potential impactors (e.g., from iron meteorites to chondrites) compared to other HSE. In addition, within this scenario the regressed HSE/Ir ratios significantly underestimate those of the impactor X, but approach those of the impactor Y. This is supported by the observation, for example relating to sample 65095, that the

regressed HSE/Ir ratios (e.g., Pd/Ir = 1.51 ± 0.36) are much lower than the ratios of subsamples (Pd/Ir = 1.72 to 4.77), but lie close to or within the range of chondrites (Table 3). The data for impact melt rock 60235 can be explained in a similar manner. Sample 60235 contains lithic clasts (Ryder and Norman, 1980) that may have been distributed unevenly among the subsamples analyzed.

Overall, for the impact melt rocks that contain more than one impactor component, the averages of the HSE ratios (including both HSE/Ir and $^{187}Os/^{188}Os$) of subsamples of each rock are utilized as the average compositions of the multiple impactors involved. In addition, with the assumption of the involvement of two impactor components, X and Y as discussed above, the highest HSE/Ir (except lowest Os/Ir) and $^{187}Os/^{188}Os$ ratios among the subsamples of each rock can be treated as the minimum (maximum for Os/Ir) estimates for the impactor X (Table 3). Similarly, the lowest HSE/Ir (highest Os/Ir) and $^{187}Os/^{188}Os$ ratios among the subsamples of each rock can be treated as the maximum estimates for the impactor Y. For example, for sample 65095 the impactor X could be close to a composition characterized by suprachondritic $^{187}Os/^{188}Os = 0.1435$, Ru/Ir = 3.29, Pt/Ir = 6.61 and Pd/Ir = 4.77, as well as subchondritic Os/Ir = 0.84, while the impactor Y might approach a HSE composition with lower $^{187}Os/^{188}Os = 0.1363$, Ru/Ir = 1.82, Pt/Ir = 2.78 and Pd/Ir = 1.72, as well as higher Os/Ir = 1.02.

5.2.3. Re-Os isotope systematics—Like previously reported HSE data for other lunar impact melt rocks (Puchtel et al., 2008; Fischer-Gödde and Becker, 2012; Sharp et al., 2014), most of the Apollo 15 and 16 impact melt rocks studied here do not show robust trends on plots of $^{187}Re/^{188}Os$ versus $^{187}Os/^{188}Os$ (Fig. 2). There are, however, significant variations in $^{187}Os/^{188}Os$ ratios of subsamples in many of these rocks. The isotopic variations primarily reflect variable ingrowth of ^{187}Os due to variations in Re/Os ratios at the time of formation, as evidenced by crude trends consistent with system closure at ~4 Ga (i.e., their formation age), as well as some variations in initial Os isotopic composition inherited from multiple impactors at the time of formation, as noted above. It is also possible that some trends reflect resetting caused by subsequent impacts.

Here we highlight the results for 67095 and 60235. For melt rock 67095,125, the data for 10 silicate fractions and 5 metal grains yield a Re-Os age of 2.97 ± 0.40 Ga (MSWD = 1.4). Unlike for sample 65095, discussed above, there is no systematic correlation between $^{187}Os/^{188}Os$ and 1/Os (Fig. 2k). This precludes an interpretation of simple two component mixing as the cause for the observed Re-Os correlation. The ^{40}Ar-^{39}Ar dating of an adjacent portion of 67095,124 yielded no plateau age, although the average incremental heating age of 3.879 ± 0.022 Ga (Fagan et al., 2013) suggests a minimum formation age that is far older than the apparent Re-Os age. The incremental heating ^{40}Ar-^{39}Ar age spectrum of 0.7 to 3.8 Ga, however, most likely indicates significant post-crystallization reheating (Fagan et al., 2013). The young Re-Os isochron age is interpreted to reflect post-formation reheating, possibly by subsequent impacts, which may have locally partially reset the Re-Os isotope systematics of this rock.

For sample 60235, interpreted to have incorporated materials from multiple impactors, part of the rock may have had comparatively recent Re addition relative to Os (and other HSE),

given the high Re/Os ratios in many subsamples of this rock (Fig. 2e). The cause for such Re addition is unclear, and it is possible that the sample was contaminated by an unknown source in the lunar environment, during collection or curation, or in the analysis. It is also possible that the isotopic composition of Re was variably modified in these samples by cosmic ray exposure, leading to errors in the isotope dilution calculations. Rhenium isotopic compositions of unspiked aliquants of samples were not determined. An increase in the $^{187}Re/^{185}Re$ ratio of a rock as a result of cosmic ray exposure, leading to calculated concentrations that appear higher than they are, can result from W burnout in samples with sufficiently high W/Re and neutron fluence. However, the W/Re of the subsamples is also unknown.

5.3. Nature of the impactor signatures

The relative concentrations of HSE in the impactors of the Apollo 15 and 16 sites are considered here by discussing data for individual samples for which there is strong evidence of two component mixing. The dominant impactor signature is also considered for those samples with multiple impactor components.

5.3.1. Apollo 15—The HSE versus Ir trends (Fig. 3), as well as their HSE patterns (Fig. EA2), of the two Apollo 15 impact melt rocks 15445 and 15455 are nearly identical, indicating that they most likely sampled the same impactor. Slight differences in their $^{187}Os/^{188}Os$ and HSE/Ir ratios can be explained by minor fractionations of Re/Os and HSE/Ir during the crystallization of both rocks. Based on field locations and available geochronological data (Alexander and Kahl, 1974; Shih et al., 1993), the two Apollo 15 impact melt rocks likely represent ejecta from the 3.91-3.94 Ga Imbrium basin-forming event (Ryder ad Bower, 1977; Ryder and Wood, 1977; Hertogen et al., 1977; Dalrymple and Ryder, 1993). As such, the HSE-rich component present in 15445 and 15455 may be derived from the Imbrium basin impactor. Except for $^{187}Os/^{188}Os$, each of these ratios is within the known range of bulk chondritic meteorites: $^{187}Os/^{188}Os$ of 0.1360 ± 0.0033, Ru/Ir (2.24 ± 0.22), Pt/Ir (2.57 ± 0.19) and Pd/Ir (2.16 ± 0.36) (Table 5). Collectively, however, this HSE composition does not overlap with any known chondrite group (Fig. 6; Fig. 7c). This may prove to be the dominant signature of the Apollo 15 site, but the data at present are too few to make this conclusion.

5.3.2. Apollo 16—Of the Apollo 16 landing site, multiple fractions of 13 impact melt rocks have now been analyzed for both HSE concentrations and Os isotopic compositions using similar methods; four samples from Fischer-Gödde and Becker (2012), and nine from this study. The data define a large range of HSE compositions that most likely indicate that this site received materials from multiple impactors (e.g., Korotev, 1994, 1996, 2000; Fischer-Gödde and Becker, 2012). As noted previously by Fischer-Gödde and Becker (2012) and verified here, the collective HSE characteristics of the various Apollo 16 impactites define generally linear trends on plots of $^{187}Os/^{188}Os$ versus HSE/Ir (Fig. 6). Each of the trends ranges from an endmember with carbonaceous chondrite-like ratios, to an endmember with considerably suprachondritic ratios, except for Os/Ir, the endmember of which is subchondritic. It should also be noted that the Apollo 15 rocks, as well as the dominant Apollo 17 impactor signature reported by Sharp et al. (2014), plot along these trends (Fig.

6). We divide the dominant HSE signatures of the diverse impactors incorporated in the Apollo 16 impactites into four groups, alphabetically defined as A, B, C and D, discussed below. These HSE-based groupings are compared with the lithophile element-based groups defined by Korotev (1994).

We did not analyze any Apollo 16 rocks with carbonaceous chondrite-like HSE compositions, but such compositions have been reported for melt or granulitic rocks from the Apollo 16 and 17 sites by Norman et al. (2002), Puchtel et al. (2008), Fischer-Gödde and Becker (2012), and Sharp et al. (2014). For example, the impactor component present in granulitic breccia 67955 (interpreted as a clast-poor, impact melt rock by Norman and Nemchin, 2014), reported by Fischer-Gödde and Becker (2012), is characterized by relative concentrations of all HSE, as well as Os isotopic composition, that are well within the range of chondritic meteorites (Fig. 6). A very similar component is also present in the polymict breccia 67915, reported by the same study. The similarity is probably due to the fact that the siderophile element budget of 67915 may be dominated by incorporated HSE-rich granulitic clasts (Ryder and Norman, 1980). Similar signatures were also observed in the Apollo 17 aphanitic melt rocks 73215 and 73255 (Puchtel et al., 2008) and 73235 (Sharp et al., 2014), each of which contained granulitic clasts, as well as the granulite 79215 (Fischer-Gödde and Becker, 2012). Collectively, these rocks (n=6), termed here as Group A (Table 5), are characterized by $^{187}Os/^{188}Os = 0.1275 \pm 0.0007$, Ru/Ir = 1.37 ± 0.16, Pt/Ir = 1.87 ± 0.32, and Pd/Ir = 0.77 ± 0.19. The relative concentrations of HSE as well as the Os isotopic composition of this component are similar to carbonaceous chondrites (Fig. 7a).

Granulitic breccias/clasts such as these are commonly characterized by formational ages of up to 4.2 Ga (Norman et al., 2007; Hudgins et al., 2008; Norman and Nemchin, 2014), yet both the granulitic impactites and clasts have coincident ^{40}Ar-^{39}Ar impact disturbance ages of ~3.9 Ga (Kirsten et al., 1973; Marti et al., 1983; Norman et al., 2007; Hudgins et al., 2008), indicating that they were excavated by the impacts that formed the lunar basins. Nevertheless, uniformity of the relative concentrations of the HSE of these rocks suggests that their HSE concentrations were not significantly overprinted by the impacts. Based on existing lithophile element data (*Lunar Sample Compendium*), 67955, 67915 and 79215 are characterized by low Sc and Sm concentrations and generally plot in the Group 4 field in the plot of Sc versus Sm (Korotev, 1994). Thus, Group A melt rocks with reported ages >4.0 Ga may belong to the Group 4 melt rocks of Korotev (1994), and are presumed to have been predominantly generated by pre-4.0 Ga impacts.

The estimated HSE compositions for the impactor components in melt rocks 60635 (3.81 ± 0.03 Ga; Deutsch and Stöffler, 1987), 63549 (3.84 ± 0.01 Ga; Norman et al., 2006) and 68416 (3.82 ± 0.01 Ga; Papanastassiou and Wasserburg, 1972; Reimold et al., 1985) are characterized by Re/Os, Ru/Ir and Pd/Ir ratios that are modestly higher than the average impactor components in the granulites, and show an affinity to enstatite and ordinary chondrite groups (Fig. 6). Given the zero y-intercepts of the HSE versus Ir trends of subsamples of each of these impact melt rocks, consistent with a single HSE-rich impactor (Fig. 3), the impactor components in these melt rocks likely did not incorporate additional granulitic materials, nor materials from other lunar basin-forming impactors. The average composition of these three rocks, termed here as Group B (Table 5), is: $^{187}Os/^{188}Os$ =

0.1297 ± 0.0007, Ru/Ir = 1.68 ± 0.05, Pt/Ir = 2.21 ± 0.37 and Pd/Ir = 1.67 ± 0.57. All of these ratios are in the range of the enstatite and ordinary chondrite groups (Fig. 7b). Collectively, these clast-poor Group B melt rocks were likely not derived from the older Imbrium impactor discussed above, but from a younger enstatite or ordinary chondrite-like impactor(s) that may have dominated in the late and post-late-stage lunar basin impact history. This interpretation is consistent with their classification as feldspathic Group 3 impactites, based on bulk lithophile element concentrations, which Korotev (1994) interpreted as formed by a post-Imbrium event(s).

The impactor components in melt rocks 62295 and 67095, termed here as Group C (Table 5), are characterized by suprachondritic $^{187}Os/^{188}Os$ (0.1349 ± 0.0018), Ru/Ir (2.01 ± 0.06), Pt/Ir (2.71 ± 0.10) and Pd/Ir (2.31 ± 0.22) ratios. They plot within the range of the two Apollo 15 rocks (Fig. 7c), and by inference, may sample the Imbrium impactor HSE fingerprint. The interpretation of an Imbrium origin is also consistent with the lithophile element concentrations of these rocks, which are also classified as mafic, KREEP-bearing Group 2 by Korotev (1994) and Fagan et al. (2013). Korotev (1994) interpreted these rocks as being associated with the Imbrium basin. Consequently, these results provide support for the conclusion that the Cayley Plains Formation, sampled by 62295 (and 60235 that is discussed below), represents ejecta deposits from the Imbrium basin (Eggleton and Schaber, 1972; Hodges et al., 1973; Ulrich, 1973). If 67095 is a fragment of the Descartes Formation (Stöffler et al., 2006), it may also confirm that the Descartes Formation originated from the Imbrium basin (Hodges et al., 1973; Ulrich, 1973; Hodges and Muehlberger, 1981; Norman et al., 2010), rather than from the older (Wilhelms, 1987; Stöffler and Ryder, 2001; Korotev et al., 2002) Nectaris event.

In contrast to the Apollo 16 impact melt rocks and granulites discussed above, the three lithic clasts extracted from regolith breccias 60016 and 65095 contain at least two impactor components with different HSE characteristics. The average HSE ratios of the impactor components in the three lithic clasts from 60016 and 65095 are indistinguishable from one another, indicating the presence of similar mixtures of impactor components. These HSE ratios are also identical, within uncertainties, to those reported by Fischer-Gödde and Becker (2012) for Apollo 16 impact melt rocks 60315 and 67935, with the exception of the Pd/Ir ratio of 60315, which is significantly higher. Collectively, the average ratios of this group of four samples, termed here as Group D (Table 5; Fig. 7d), are $^{187}Os/^{188}Os$ = 0.1387 ± 0.0019, Ru/Ir = 2.46 ± 0.20, Pt/Ir = 3.13 ± 0.36, and Pd/Ir = 3.35 ± 1.16. The latter ratio is highly variable among subsamples, with ratios ranging from 2.9 to 4.4. All ratios are higher (except lower Os/Ir) than for all other known lunar impact rocks (Fig. 6; Fig. 7).

The high HSE/Ir ratios of the Group D rocks imply incorporation of more fractionated impactor materials than the other HSE groups, including the Group C Imbrium signature. Of note, based on the lithophile element concentrations, the clasts from 60016 and 65095, and melt rock 60315, fall into the lithophile element compositional Group 1 (60016 and 60315) or 2 (65095) defined by Korotev (1994) that have been suggested to have been derived from the Imbrium region (e.g., Korotev, 1994, 1996, 2000). However, their formation ages range from Imbrium-like (60016,286 and 65095; Table 1) to significantly older (60016,290 and 60315; Table 1). Given that the aforementioned Group C rocks are also classified as

the lithophile element compositional Group 2, if sample 65095 contains Imbrium impactor material as the Group C rocks, its HSE signature described above demands another older, more fractionated component than the Imbrium impactor, such as that recorded by sample 67935, the 4.21 ± 0.13 Ga Group D melt rock. Likewise, a similar conclusion is made for the Group 1 rocks 60016 and 60315.

Despite it having multiple impactor components, the dominant impactor signature in sample 60235 is similar in its HSE ratios to those of Group C (including samples 62295 and 67095). This implies that the HSE budget of 60235 was primarily controlled by impactor materials from the Imbrium basin, like 62295 and 67095 discussed above. Consequently, the HSE ratios of the dominant impactor signature in 60235 are incorporated into Group C (Table 5).

Collectively, the impactites in the Apollo 16 site appear to document the HSE signatures of multiple, diverse impactors ranging from chondritic to suprachondritic HSE compositions over a considerable period of time from pre-4.0 Ga (at least up to 4.2 Ga) to ~3.8 Ga.

5.4. Comparison with other lunar impact rocks

5.4.1. Apollo 14—To date, two Apollo 14 impact rocks have been analyzed for both HSE concentrations and Os isotopic compositions: impact melt rock 14310 (Fischer-Gödde and Becker, 2012) and polymict melt breccia 14321 (Puchtel et al., 2008). Polymict breccia 14321 was collected from near the edge of the Cone Crater and is generally interpreted to be part of the Fra Mauro Formation (Wilshire and Jackson 1972; Swann et al., 1972, 1977). Despite it containing materials derived from several local impacts (Duncan et al., 1975; Grieve et al., 1975), the subsamples of 14321 are characterized by well-defined HSE versus Ir trends with zero y-intercepts (Puchtel et al., 2008), suggesting the presence of a single HSE-rich dominant impactor in this rock. The HSE characteristic of this impactor ($^{187}Os/^{188}Os$ = 0.1341 ± 0.0010, Ru/Ir = 2.00 ± 0.15, Pt/Ir = 2.69 ± 0.23, and Pd/Ir = 1.92 ± 0.34; Table 5) is consistent with the inferred Imbrium impactor composition defined by the Apollo 15 impact rocks (Fig. 7c). This observation supports the conclusion that the Fra Mauro Formation, sampled by 14321, was primary ejecta of the Imbrium basin-forming impact (Duncan et al., 1975), rather than locally derived material excavated by a secondary impact(s) related to the Imbrium event (Hawke and Head, 1977).

The provenance of melt rock 14310 is poorly constrained because it was found on the surface as a separate sample. It may or may not have originated from the Fra Mauro Formation. The meteoritic impactor component present in 14310 is characterized by slightly higher $^{187}Os/^{188}Os$ (0.1311 ± 0.0003), Ru/Ir (1.78 ± 0.03), Pt/Ir (2.37 ± 0.03) and Pd/Ir (1.68 ± 0.18) ratios than the averages of the major chondrite groups (Table 5; Fig. 6). However, as shown in Fig. 6, the HSE signature of this impactor component is not consistent with the Imbrium impactor composition, but is instead similar to that of the Apollo 17 poikilitic melt rocks that are discussed below (Table 5; Fig. 7e; Sharp et al., 2014). Along with the ^{40}Ar-^{39}Ar plateau ages (3.89 ± 0.04 to 3.91 ± 0.05 Ga; Turner et al., 1971; York et al., 1972) reported for the rock, this indicates that impact melt rock 14310 was not derived from the Fra Mauro Formation, but instead may have formed at a time coincident with the creation of the Serenitatis basin.

5.4.2. Apollo 17—The Apollo 17 poikilitic melt rocks are commonly concluded to represent ejecta of the Serenitatis basin-forming impact (Spudis and Ryder, 1981; Dalrymple and Ryder, 1996). Because these rocks are melt-rich and clast-poor, and contain few HSE-rich granulitic clasts in their clast populations, their comparable HSE characteristics are interpreted to reflect the composition of the impactor responsible for the Serenitatis basin (Puchtel et al., 2008; Sharp et al., 2014), here referred to as the Serenitatis impactor. As illustrated in Fig. 6, the Serenitatis impactor is also characterized by modestly suprachondritic $^{187}Os/^{188}Os$ (0.1322 ± 0.0013), Ru/Ir (1.87 ± 0.30), Pt/Ir (2.36 ± 0.31) and Pd/Ir (1.85 ± 0.41), relative to known chondrite groups (Table 5; Sharp et al., 2014), but to a lesser extent compared to the Imbrium impactor (Fig. 7c and e). In addition to materials from the Serenitatis impactor, some Apollo 17 aphanitic melt breccias also contain abundant HSE-rich granulitic breccia clasts that dominate the HSE signature (Puchtel et al., 2008; Sharp et al., 2014), as discussed above. Collectively, the Apollo 17 impact melt rocks not only incorporate materials from the Serenitatis impactor, characterized by suprachondritic $^{187}Os/^{188}Os$, Ru/Ir, Pt/Ir and Pd/Ir ratios, but also reflect the existence of a pre-Serenitatis impactor(s) with a chondritic relative HSE composition (Fischer-Gödde and Becker, 2012).

5.4.3. Lunar meteorites—At present, two lunar impact melt meteorites derived from unknown locations have been analyzed for both HSE concentrations and Os isotopic compositions: regolith breccia DaG 400 and melt rock NWA 482. The breccia DaG 400 is composed of a fine-grained matrix with subophitic clasts of melt breccias, granulitic fragments, recrystallized anorthositic clasts and other mineral fragments (Zipfel et al., 1998). The subsamples of this melt rock chip are characterized by moderate HSE concentrations (e.g., Ir = 2.5 to 4.0 ng/g) and generally well-defined HSE versus Ir trends with y-intercepts of essentially zero (Fischer-Gödde and Becker, 2012). Given that the averaged $^{187}Os/^{188}Os$ and slope-derived HSE/Ir ratios ($^{187}Os/^{188}Os$ = 0.1290 ± 0.0014, Ru/Ir = 1.83 ± 0.25, Pt/Ir = 2.1 ± 0.6, and Pd/Ir = 1.33 ± 0.19; Table 5) are greater than those of granulitic impactites discussed above, this indicates that the rock chip analyzed contained little HSE-rich granulitic fragments, and primarily records a single HSE-rich dominant impactor component that is characterized by a chondritic relative HSE compositions similar to those of the Apollo 16 Group B impact melt rocks 60635, 63549, and 68416 (Fig. 7b). Similar HSE data are observed in the other lunar meteorite NWA 482 that does not contain any large clasts of target rocks (Puchtel et al., 2008). Along with the Apollo 16 Group B melt rocks, the two lunar meteorites are younger (~3.75 Ga for NWA 482, Daubar et al., 2002; and <3.8 Ga for DaG 400, Cohen et al., 2005) than the major impact melt rocks formed by the lunar basin-forming impacts (~4.0 to 3.86 Ga). This suggests that the two lunar meteorites and the Apollo 16 Group B impact melt rocks were derived from later (<3.84 Ga) impact events by impactors with essentially chondritic HSE composition.

5.5. Origin of HSE characteristics in lunar impact melt rocks

5.5.1 Models to generate HSE signatures—Of the lunar impact melt rocks studied to date, the collective HSE data define a generally linear trend on plots of $^{187}Os/^{188}Os$ versus HSE/Ir, ranging from an endmember composition with carbonaceous chondrite-like ratios, to an endmember with suprachondritic ratios in all HSE ratios, except for subchondritic Os/Ir (Fig. 6). By and large, those impact rocks showing essentially chondritic

HSE signatures (e.g., Apollo 16 Group A and B samples), can be straightforwardly interpreted to have been derived from impactors that had HSE compositions similar to known chondrite groups (Fig. 7; Puchtel et al., 2008; Fischer-Gödde and Becker, 2012). However, the HSE signatures of impact melt rocks with mostly suprachondritic HSE/Ir ratios (e.g., Apollo 15, and Apollo 16 Group C and D samples) could not have been made through the mixing of known chondritic impactors. Possible scenarios to explain the observed trends towards the suprachondritic HSE/Ir (except subchondritic Os/Ir) ratios are discussed below.

One means to explain the apparently non-chondritic HSE characteristics of some lunar impactors is to appeal to bulk planetesimals with compositions outside the range currently sampled by Earth today. There are considerable variations in the relative concentrations of HSE among chondrites, particularly with regard to Re/Os, Ru/Ir and Pd/Ir (Horan et al., 2003; Fischer-Gödde et al., 2010). The causes of the variations in the relative concentrations of the HSE among chondrites are not well understood, so the extent to which the HSE may have been fractionated in a much larger sampling of early-formed planetesimals is currently impossible to assess. As shown in Fig. 6, there are individual chondrites with bulk characteristics that can match the extent of HSE/Ir and $^{187}Os/^{188}Os$ variations included in Groups A, B and C. Consequently, it is clear that either nebular and/or parent body processes can produce such variations, although no single chondrite has the complete HSE profile of, for example, Group C.

Group D is noteworthy in that the endmember characteristics of this group are well beyond the range of known chondrites with respect to Ru/Ir, Pt/Ir, Pd/Ir, $^{187}Os/^{188}Os$ and Os/Ir. In order to appeal to a planetesimal with this composition, it requires that the bulk impactor was constructed of materials that underwent nebular or parent body processes leading to far greater fractionation of some HSE ratios than those recorded in sampled chondrites. Although this is possible, unless bulk chondrites with such extremely fractionated HSE are discovered, appealing to such an impactor will remain highly speculative.

Another option to account for the more fractionated HSE characteristics of some impact melt rocks is to assume that the impactor consisted of, or contained a substantial proportion of evolved metal (e.g., Korotev, 1994; Fischer-Gödde and Becker, 2012). Solid metal-liquid metal fractionation under certain circumstances can drive HSE ratios from chondritic towards the ratios observed in Group D, including lowered Os/Ir, and beyond. The trend produced by the fractional crystallization sequence of a metallic core recorded by group IVA iron meteorites is shown for comparison with the lunar data in Fig. 6. Despite the lack of a perfect fit to all of the trends recorded by the collective lunar impact melt rocks, the sequence qualitatively accounts for the changes in HSE ratios in a way that variations within the individual chondrite groups do not. As noted by Sharp et al. (2014), however, there are some physical plausibility issues with respect to models that involve fractionated planetesimal cores. The relative concentrations of HSE in bulk asteroidal cores are most likely within the chondritic range. Thus, for basin-size events, such models require a sizable planetesimal core to partially or completely crystallize, then the core must be broken up in such a manner to isolate and access the minor portion of the core that would have the characteristics of an appropriately evolved meteorite.

In order to further investigate the possibility of impact contributions from chemically evolved metals, we consider two options. In the first, we envision individual basins formed as a result of the impact of differentiated impactors characterized by wholly chondritic bulk compositions. For this scenario, metal with fractionated HSE compositions present in portions of the respective impactor cores would be separated by the impacts and differentially distributed into impact-generated melts. It has been suggested, for example, that the Imbrium basin was produced by an impactor moving from northwest to southeast, and that the projectile may have been decapitated (e.g., Schultz et al., 2012). Fragments of the projectile have been implicated in downrange lunar surface sculpture (Schultz, 2001), so some of that debris may have been incorporated into melts in downrange sites, such as the Apollo 16 site. In a recent hydrocode model of the larger South Pole-Aitken basin impact event (Wieczorek et al. 2012), a differentiated projectile hitting at an angle of 45 degrees was assumed. In that model, the silicate mantle of the impactor was largely vaporized, and the remaining fraction of the mantle and 80% of the core were deposited in the lunar crust downrange of the impact. The model did not have the resolution necessary to determine if different parts of a fractionated core could have been separated to produce chemically distinct impact melt products with fractioned compositions, but such an occurrence is conceivable. If decapitation processes occurred in smaller basin-forming events, like Imbrium and Serenitatis, then it might be imagined that the metal fraction in or near the basin might complement the metal fraction carried downrange. With the current analytical resolution, we do not see the type of complementary signatures that might be expected when comparing samples proximal to the basin rim (15445 and 15455) and those in more distal ejecta deposits (e.g., 60235, 62295 and 67095), so this interpretation must remain highly speculative at present.

As a second option involving a metallic impactor we consider the model of Fischer-Gödde and Becker (2012). That study appealed to mixing between an evolved iron meteorite impactor and an earlier-formed chondritic impactor signature to generate the most extreme compositions observed in Apollo 16 impact melt rocks. Our new results provide some additional support for this type of model. The presumed exogenous metal grains from Apollo 16 Group C melt rock 67095 are characterized by prominent depletions in moderately volatile siderophile elements. For example, Ga Ge and Zn are depleted by approximately one, two and three orders of magnitude respectively, as compared with bulk chondrites (Fig. 4). Given the presence of abundant, large (~300 μm) troilite crystals in the melt rock, indicating a S-rich vapor plume (a volatile element) during impact, the depletions of moderately volatile siderophile elements in these metal grains cannot be explained to be a result of volatility-controlled fractionation processes during impact and melt sheet evolution on the Moon. Comparable degrees of Ga and Ge (and perhaps Zn) depletions, as well as similar relative HSE concentrations (Fig. 8), are seen in some group IVA iron meteorites (Fig. EA6; e.g., Schaudy et al., 1972; McCoy et al., 2011). Thus, the depletions of Ga and Ge may have been inherited from the impactor that, like the IVA irons, had been depleted in these elements prior to impact, for example by metal-silicate segregation in the parent body under oxidizing conditions (McCoy et al., 2011). The accompanying fractionations in HSE could then reflect solid metal-liquid metal fractionation as a consequence of core crystallization. For example, the metal grains from sample 67095 have Os isotopic

compositions ($^{187}Os/^{188}Os = 0.1369 \pm 0.0021$) and relative HSE concentrations (Ru/Ir = 1.99 ± 0.08, Pt/Ir = 2.96 ± 0.43, and Pd/Ir = 2.27 ± 0.24) that are identical, within uncertainties, to those of the IVA iron meteorite Charlotte ($^{187}Os/^{188}Os = 0.1347$, Ru/Ir = 1.989, Pt/Ir = 3.051, and Pd/Ir = 2.286; McCoy et al., 2011).

These lines of evidence suggest that the 67095 metal could have been derived from an isolated, evolved portion of a group IVA-like planetesimal core, with an average siderophile element composition similar to that of the IVA iron meteorite Charlotte. If this interpretation is correct, the dominant HSE signature of the Apollo 16 Group C impact melt rocks (and possibly the Apollo 15 impact melt rocks) may have been inherited from an Imbrium basin-forming impactor, which originated as an evolved portion of a planetesimal core (Fig. 7c).

The more strongly suprachondritic HSE characteristics of the Apollo 16 Group D melt rocks are also consistent with the incorporation of impactor metals. For instance, the two metal grains from clast 60016,290b show higher HSE ratios ($^{187}Os/^{188}Os = 0.1386 \pm 0.0004$, Ru/Ir = 2.27 ± 0.02, and Pd/Ir = 2.86 ± 0.26; except for overlapping Pt/Ir = 2.99 ± 0.28) than those of Charlotte, and their relative HSE concentrations plot between Charlotte and another more fractionated IVA iron meteorite, Bushman Land ($^{187}Os/^{188}Os = 0.1394$, Ru/Ir = 2.64, Pt/Ir = 4.33 and Pd/Ir = 4.84; McCoy et al., 2011; Fig. 7d). Given that the Apollo 16 Group D samples most likely contained multiple impactor components, their HSE signatures can be accounted for by the mixing of the putative Imbrium impactor (Group C from above), or carbonaceous chondrite-like impactor (Joy et al, 2012; Fischer-Gödde and Becker, 2012), with a more fractionated, Bushman Land-like impactor component. Such an interpretation requires the incorporation of two distinct but similarly fractionated portions of the same impactor core. The fact that the more fractionated component is primarily found as metal in clasts that are embedded in a younger matrix requires that the two components impacted the Moon at different times. Consequently, the coincidences necessary to account for these features are substantial.

Fischer-Gödde and Becker (2012) used the above arguments to conclude that the HSE trends present in the HSE data for the Apollo 16 suite can be accounted for by a more simple, two component mixing scenario. They argued for mixing between a carbonaceous chondrite-like component (sampled by granulitic clasts that are older than 4.0 Ga), and an evolved IVA iron meteorite-like component similar to Bushman Land, sampled most directly by 60315 and 67935. As noted, Fischer-Gödde and Becker (2012) reported a Re-Os isochron age of ~4.21 ± 0.13 Ga for sample 67935. This age is in good agreement with a similar Sm-Nd isochron age of 4.20 ± 0.07 Ga for sample 67955, a noritic anorthosite taken from the same boulder (Norman et al., 2007; Norman and Nemchin, 2014). Thus, for their model both endmember components appear to predate the formation of the late-stage basins, such as Imbrium and Serenitatis. Samples with ratios intermediate between the two endmembers, including metals such as those from 67095, would have formed through the mixing of the two components in the evolving melt sheet. Consistent with this, efficient homogenization of two or more impactor components in melt rocks, followed by irregular distribution of the HSE hosts within the rocks, can result in linear HSE versus Ir trends with zero y-intercepts.

Given that both of the two endmember components in this model predate the later basin forming events, Fischer-Gödde and Becker (2012) boldly argued that the HSE signatures of other lunar impact melt rocks that plot along the HSE trends (Apollo 17 dominant, Apollo 14, lunar meteorites) might also be the result of the mixing of the same two component. If this was a global event, then the later, basin-forming events mixed the two components either without substantially adding fresh HSE to the mixtures or adding a third component that was similar to one of the other two.

We offer a minor modification to the Fischer-Gödde and Becker (2012) model which may solve some of the plausibility issues. Rather than attempt to account for the evolved component as a fragment of a solidified core, we instead envision the component to have originated from the evolved metallic liquid present in a solidifying core, which was separated from the solidified portion of the core, for instance, by a hit-and-run collision (e.g., Asphaug et al., 2006), most likely during the first several Myr of the solar system history (e.g., Bottke et al. 2006). The Group IVA irons, for example, may have been produced in a relatively large core (150 ± 50 km in radius) that was stripped of its silicate mantle by one of these collisions (Yang et al. 2007, 2008; Goldstein et al. 2014). A good fit to the required endmember composition (for example, the subsample 65095_D that has the extreme HSE composition characterized by $^{187}Os/^{188}Os$ = 0.1435, Re/Ir = 0.108, Ru/Ir = 3.29, Pt/Ir = 4.85 and Pd/Ir = 4.77, as well as Os/Ir = 0.838 calculated from Table 2; CI normalized values are shown in Fig. 7d) can be achieved for most ratios via ~54% fractional crystallization of a core with chondritic relative concentrations of HSE and initially 4 wt.% S and 0.1 wt.% P (see modeling detail in the Electronic Annex). The resulting Pd/Ir of the model liquid is substantially higher (7.3) than any of the impact melt rocks, but the solid metal-liquid metal distribution coefficient for Pd is the least certain of the elements modeled (e.g., Walker et al., 2008). Our model utilizes the same parameterization to obtain distribution coefficients as was applied to the IVA iron meteorite system by McCoy et al. (2011), although this model assumes 4 wt.% as the initial S rather than the 3% preferred for the IVA system by McCoy et al. This liberated metal could then go on to crystallize to form a planetesimal that eventually became a major lunar impactor (e.g., Bottke et al. 2006).

It will ultimately be necessary to examine the genetics of the lunar impactors using nucleosynthetic variations in elements, such as Ru (e.g., Chen et al., 2010), to assess whether or not a very limited number of impactors can account for the range of HSE concentrations present in impact melt rocks.

5.5.2 Impactors and time—Two key issues regarding the formation of the lunar basins are the period of time over which the basins were generated, and whether or not the compositions of the impactors varied in a way that relates to timing and/or location of their origins. With regard to the latter issue, it has been commonly argued that the basin-forming impactors originated from what is now the asteroid belt, based on geochemical (Kring and Cohen, 2002), geological (Strom et al., 2005; Marchi et al. 2012), and mineralogical (Joy et al. 2012) evidence. This conclusion may also be consistent with dynamical models of the early solar system and their effect on evolving asteroid and cometary populations (e.g., Gomez et al., 2005; Morbidelli 2010; Walsh et al., 2011).

The compilation of HSE data and chronological data for lunar impact melt rocks presented here does not reveal any obvious composition versus age trends (Fig. 9). Apollo 16 Group A samples with ages of 4 Ga or older, have carbonaceous chondrite affinities. Group B samples and lunar meteorites (DaG 400 and NWA 482) are characterized by ages younger than 3.84 Ga and have enstatite and ordinary chondrite affinities. This could be interpreted to mean that the flux of impactors was initially dominated by carbonaceous chondritic-like compositions. These impactors may even have preceded the putative late heavy bombardment. The late-stage impactors of Group B are characterized by compositions similar to ordinary and enstatite chondrites. However, as with all studies of the chronology of lunar impact melt rocks, it remains unknown which of the ages, if any, reflect that of the primary, basin-forming impact that created the rock. It has been repeatedly suggested that at least some ages are partially or wholly reset as a result of later impacts (e.g., Norman et al., 2006; Fernandes et al., 2013).

The impactors with more fractionated HSE characteristics, e.g., Groups C and D of the Apollo 16 suite, are more difficult to fit into an age sequence. Highly-fractionated impact melt rocks have ages that are both old, such as the ~4.2 Ga sample 67935 from Fischer-Gödde and Becker (2012), presumably predating the putative late heavy bombardment, and melt rocks with an intermediate age of ~3.9 Ga, such as the lithic clasts from 60016 and 65095. If these ages reflect true formational ages resulting from basin-forming impacts, then the impacting flux was highly variable in composition as time progressed.

The two component model of Fischer-Gödde and Becker (2012) circumvents some timing issues by calling on both major components to be added to the lunar crust prior to the formation of the later stage basins. This model requires that most of the ages determined for these rocks are reset ages. This model, however, could face challenges if any of the HSE signatures can ultimately be tied to a true Imbrium or Serenitatis formational age.

6. CONCLUSIONS

1) Concentrations of highly siderophile elements, as well as Os isotope compositions, indicate diverse impactor components for Apollo 15 and 16 impact melt rocks. These impactor components range from chondritic to suprachondritic $^{187}Os/^{188}Os$, Ru/Ir, Pt/Ir and Pd/Ir ratios. Collectively, the inferred impactor components from this study, as well as compositional data for most other lunar impact melt rocks form linear trends on plots of HSE/Ir versus $^{187}Os/^{188}Os$.

2) While the chondritic HSE signatures are interpreted to have been derived from impactors that had HSE compositions similar to known chondrite groups, the more fractionated HSE characteristics could not have been made by mixing of known chondritic impactors. They must instead reflect either contributions from early solar system bodies with previously unknown chemical compositions, or preferential incorporation of evolved metallic materials separated from a fractionated planetesimal core.

3) The collective database for HSE and impact melt rock ages suggests that impactors with both chondritic and fractionated relative HSE concentrations added substantial HSE to the lunar crust prior to the later-stage basin-forming impacts, such as Imbrium and Serenitatis.

4) One possible interpretation for global HSE ratio trends, previously suggested by Fischer-Gödde and Becker (2012), is that the later-stage basin-forming impacts were more important with respect to mixing prior impactor components into melt rocks, rather than contributing much to the HSE budgets of the rocks themselves.

Supplementary Material

Refer to Web version on PubMed Central for supplementary material.

ACKNOWLEDGEMENTS

This work was supported by NASA NLSI, Astrobiology and SSERVI grants NNA09DB33A, NNX09AJ20A and NNA14AB07A, respectively. This support is gratefully acknowledged. We are also grateful for the thoughtful and constructive reviews by Mario Fischer-Gödde, Randy Korotev, Associate Editor Christian Koeberl, and Executive Editor Marc Norman.

8. REFERENCES

Achterbergh EV, Ryan CG, Jackson SE and Griffin WL (2001) Appendix 3: data reduction software for LA-ICP-MS. In Laser Ablation-ICP-MS in the Earth Sciences, vol. 29 (ed. Sylvester P). Mineralogical Association of Canada, Short Course Series, 243pp.

Albarede F, Ballhaus C, Blichert-Toft J, Lee CT, Marty B, Moynier F and Yin QZ (2013) Asteroidal impacts and the origin of terrestrial and lunar volatiles. Icarus 222, 44–52.

Alexander EC and Kahl SB (1974) ^{40}Ar-^{39} Ar studies of lunar breccias. Proc. Lunar Sci. Conf 5, 1353–1373.

Anders E, Ganapathy R, Krähenbühl U and Morgan JW (1973) Meteoritic material on the Moon. Moon 8, 3–24.

Andrews-Hanna JC and Zuber MT (2010) Elliptical craters and basins on the terrestrial planets. Large Meteorite Impacts & Planetary Evolution 465, 1–13.

Asphaug E, Agnor CB and Williams Q (2006) Hit-and-run planetary collisions. Nature 439, 155–160. [PubMed: 16407944]

Axon HJ and Goldstei Ji (1973) Metallic particles of high cobalt content in Apollo-15 soil samples. Earth Planet. Sci. Lett 18, 173–180.

Bernstein ML (1983) 15445 and 15455: Origin and preliminary age data. Lunar Planet. Sci. Conf. XIV. Lunar Planet. Inst., Houston. 33–34 (abstr.).

Birck JL, RoyBarman M and Capmas F (1997) Re-Os isotopic measurements at the femtomole level in natural samples. Geostandard Newslett. 21, 19–27.

Boynton WV, Chou CL, Robinson KL, Warren PH and Wasson JT (1976) Lithophiles, siderophiles and volatiles in Apollo 16 soils and rocks. Proc. Lunar Sci. Conf 7, 727–742.

Bottke WF, Nesvorný D, Grimm RE, Morbidelli A, and O'Brien DP (2006) Iron meteorites as remnants of planetesimals formed in the terrestrial planet region. Nature 439, 821–824. [PubMed: 16482151]

Brandon AD, Humayun M, Puchtel IS, Leya I and Zolensky M (2005) Osmium isotope evidence for an s-process carrier in primitive chondrites. Science 309, 1233–1236. [PubMed: 16109878]

Brandon AD, Humayun M, Puchtel IS and Zolensky ME (2005) Re-Os isotopic systematics and platinum group element composition of the Tagish Lake carbonaceous chondrite. Geochim. Cosmochim. Acta 69, 1619–1631.

Cadogan PH and Turner G (1976) The chronology of the Apollo 17 Station 6 boulder. Proc. Lunar Sci. Conf 7, 2267–2285.

Campbell AJ and Humayun M (2005) Compositions of group IVB iron meteorites and their parent melt. Geochim. Cosmochim. Acta 69, 4733–4744.

Chen JH, Papanastassiou DA and Wasserburg GJ (1998) Re-Os systematics in chondrites and the fractionation of the platinum group elements in the early solar system. Geochim. Cosmochim. Acta 62, 3379–3392.

Cohen AS and Waters FG (1996) Separation of osmium from geological materials by solvent extraction for analysis by thermal ionisation mass spectrometry. Analytica Chimica Acta 332, 269–275.

Cohen BA, Swindle TD and Kring DA (2005) Geochemistry and ^{40}Ar-^{39}Ar geochronology of impact-melt clasts in feldspathic lunar meteorites: Implications for lunar bombardment history. Meteoritics & Planetary Science 40, 755–777.

Compston W, Foster JJ and Gray CM (1977) Rb—Sr systematics in clasts and aphanites from consortium breccia 73215. Proc. Lunar Sci. Conf 8, 2525–2549.

Dalrymple GB and Ryder G (1993) ^{40}Ar/^{39}Ar age spectra of Apollo 15 impact melt rocks by laser step-heating and their bearing on the history of lunar basin formation. J. Geophys. Res. Planet 98, 13085–13095.

Dalrymple GB and Ryder G (1996) ^{40}Ar/^{39}Ar age spectra of Apollo 17 highlands breccia samples by laser step heating and the age of the Serenitatis basin. J. Geophys. Res. Planet 101, 26069–26084.

Daubar IJ, Kring DA, Swindle TD and Jull AJT (2002) Northwest Africa 482: A crystalline impact-melt breccia from the lunar highlands. Meteorit. Planet. Sci 37, 1797–1813.

Deutsch A and Stöffler D (1987) Rb-Sr analyses of Apollo-16 melt rocks and anew age estimate for the Imbrium Basin - Lunar basin chronology and the early heavy bombardment of the Moon. Geochim. Cosmochim. Acta 51, 1951–1964.

Dowty E, Keil K and Prinz M (1974) Igneous rocks from Apollo 16 rake samples. Proc. Lunar Planet. Sci. Conf 5, 431–445.

Duncan AR, Mckay SM, Stoeser JW, Lindstrom MM, Lindstrom DJ, Fruchter JS and Goles GG (1975) Lunar polymict breccia-14321 - compositional study of its principal components. Geochim. Cosmochim. Acta 39, 247–260.

Eggleton RE and Schaber GG (1972) Cayley Formation interpreted as basin ejecta. In *Apollo 16 Prelim. Sci. Rep.* NASA SP-135, pp. 29–7 to 29–16.

Fagan AL, Neal CR, Beard SP and Swindle TD (2013) Bulk composition and ^{40}Ar-^{39}Ar age dating suggests impact melt sample 67095 may be exotic to the Apollo 16 site. Lunar Planet. Sci. XLIV. Lunar Planet. Inst., Houston. #3075 (abstr.).

Fernandes VA, Fritz J, Weiss BP, Garrick-Bethell I, Shuster DL (2013) The bombardment history of the Moon as recorded by ^{40}Ar-^{39}Ar chronology. Meteorit. Planet. Sci 48, 241–269.

Fischer-Gödde M and Becker H (2012) Osmium isotope and highly siderophile element constraints on ages and nature of meteoritic components in ancient lunar impact rocks. Geochim. Cosmochim. Acta 77, 135–156.

Fischer-Gödde M, Becker H and Wombacher F (2010) Rhodium, gold and other highly siderophile element abundances in chondritic meteorites. Geochim. Cosmochim. Acta 74, 356–379.

Ganapathy R, Morgan JW, Krähenbühl U and Anders E (1973) Ancient meteorite components in the lunar highlands rocks: Clues from trace elements in Apollo 15 and 16 samples. Proc. Lunar Sci. Conf 4, 1239–1261.

Gnos E, Hofmann BA, Al-Kathiri A, Lorenzetti S, Eugster O, Whitehouse MJ, Villa I, Jull AJT, Eikenberg J, Spettel B, Krähenbühl U, Franchi IA, and Greenwood GC (2004) Pinpointing the source of a lunar meteorite: Implications for the evolution of the Moon. Science 305, 657–659. [PubMed: 15286369]

Goldstein JI, Axon HJ, and Agrell SO (1972) The grape cluster, metal particle 63344,1. Earth Planet. Sci. Lett 28, 217–224.

Goldstein JI, Yang J, and Scott ERD (2014) Determining cooling rates of iron and stony-iron meteorites from measurements of Ni and Co at kamacite-taenite interfaces. Geochim. Cosmochim. Acta 140, 297–320.

Gomes R, Levison HF, Tsiganis K and Morbidelli A (2005) Origin of the cataclysmic Late Heavy Bombardment period of the terrestrial planets. Nature 435, 466–469. [PubMed: 15917802]

Gooley RC, Brett R and Warner JL (1973) Crystallization history of metal particles in Apollo 16 rake samples. Proc. Lunar Sci. Conf 4, 799–810.

Grieve RA, Mckay GA, Smith HD and Weill DF (1975) Lunar polymict breccia-14321 - petrographic study. Geochim. Cosmochim. Acta 39, 229–245.

Gros J, Takahashi H, Hertogen J, Morgan JW and Anders E (1976) Composition of the projectiles that bombarded the lunar highlands. Proc. Lunar Sci. Conf, 7(2), 2403–2425.

Hawke BR and Head JW (1977) Local vs. Imbrium basin material at the Apollo 14 site: Some observations and suggestions. In Interdisciplinary Studies by the Imbrium Cosortium, v.2 (Wood JA, ed.), LSI Contr. No. 268D, p. 91–96. Center for Astrophysics, Cambridge.

Head JW (1974) Stratigraphy of the Descartes region (Apollo 16): Impliations for the origin of smaples. Moon 11, 77–99.

Hertogen J, Janssens MJ, Takahashi H, Palme H and Anders E (1977) Lunar basins and craters: evidence for systematic compositional change of bombarding population. Proc. Lunar Sci. Conf 8(1), 17–45.

Higuchi H and Morgan JW (1975) Ancient meteoritic component in Apollo 17 boulders. Proc. Lunar Sci. Conf 6(2), 1625–1651.

Hodges CA (1972) Geological map of part of the Descartes region of the Moon. *Geologic Atlas of the Moon.* Part of the Descartes region-Apollo 16. USGS Map I-748 Part 2. Scale 1:50000.

Hodges CA and Muehlberger WR (1981) Summary and critique of geologic hypotheses, *Geology of the Apollo 16 Area, Central Lunar Highlands*. U.S. Geol. Survey Prof. Paper 1048, 215–230.

Hodges CA, Muehlberger WR and Ulrich GE (1973) Geologic setting of Apollo 16. *Proc.Lunar Sci. Conf.***4**, *Geochim. Cosmochim. Acta*, 1 (Suppl. 4), 1–25.

Horan MF, Walker RJ, Morgan JW, Grossman JN and Rubin AE (2003) Highly siderophile elements in chondrites. Chem. Geol 196, 5–20.

Hubbard NJ, Rhodes JM, Gast PW, Bansal BM, Shih CY, Wiesmann H and Nyquist LE (1973) Lunar rock types: The role of plagioclase in non-mare and highland rock types. Proc. Lunar Sci. Conf 4, 1297–1312.

Hudgins JA, Spray JG, Kelley SP, Korotev RL and Sherlock SC (2008) A laser probe $_{40}$Ar/$_{39}$Ar and INAA investigation of four Apollo granulitic breccias. Geochim. Cosmochim. Acta 72, 5781–5798.

Huneke JC, Jessberger EK, Podosek FA and Wasserburg GJ (1973) 40Ar/39Ar measurements in Apollo 16 and 17 samples and the chronology of metamorphic and volcanic activity in the Taurus-Littrow region. Proc. Lunar Sci. Conf 4, 1725–1756.

Hunter RH and Taylor LA (1981) Rust and schreibersite in Apollo 16 highland rocks: Manifestations of volatile-element mobility. Proc. Lunar Planet. Sci. Conf 12, 253–259.

James OB (2002) Distinctive meteoritic components in lunar “cataclysm” impact melt breccias. Lunar Planet. Sci. XXXIII, #1210 (abstr.).

James OB, Ash RD, McDonough WF, Puchtel IS and Walker RJ (2007) Fractionation and volatile redistribution of siderophile elements in metal grains from lunar impact melt breccia 76215. Lunar Planet. Sci. XXXVIII, #1094 (abstr.).

Jessberger EK, Staudacher T, Dominik B and Kirsten T (1978) Argon—argon ages of aphanite samples from consortium breccia 73255. Proc. Lunar Planet. Sci. Conf 9, 841–854.

Joy KH, Kring DA, Bogard DD, McKay DS and Zolensky ME (2011) Re-examination of the formation ages of the Apollo 16 regolith breccias. Geochim. Cosmochim. Acta 75, 7208–7225.

Joy KH, Zolensky ME, Nagashima K, Huss GR, Ross DK, McKay DS, and Kring DA (2012) Direct detection of projectile relics from the end of the lunar basin-forming epoch. Science 336, 1426–1429. [PubMed: 22604725]

Kirsten T, Horn P and J. K (1973) ^{39}Ar–^{40}Ar dating and rare gas analysis of Apollo 16 rocks and soils. *Proc. Lunar Sci. Conf.***4**, *Geochim. Cosmochim. Acta* 2 (Suppl. 4), 1757–1784.

Kirsten T and Horn P (1974) Chronology of the Taurus-Littrow region III: ages of mare basalts and highland breccias and some remarks about the interpretation of lunar highland rock ages. Proc. Lunar Sci. Conf 5, 1451–1475.

Koeberl C (1998) Identification of meteoritic component in impactites. In: Grady MM, Hutchison R, McCall GJH, Rothery D (Eds.), *Meteorites: Flux with Time and Impact Effects*, Geological Society, London, Special Publications, v. 140, pp. 133–153.

Korotev RL (1987) The meteorite component of Apollo-16 noritic impact melt breccias. J. Geophys. Res. Solid Earth Planet 92, E491–E512.

Korotev RL (1994) Compositional variation in Apollo-16 impact-melt breccias and inferences for the geology and bombardment history of the central-highlands of the Moon. Geochim. Cosmochim. Acta 58, 3931–3969.

Korotev RL (1996) On the relationship between the Apollo 16 ancient regolith breccias and feldspathic fragmental breccias, and the composition of the prebasin crust in the Central Highlands of the Moon. Meteorit. Planet. Sci 31, 403–412.

Korotev RL (2000) The great lunar hot spot and the composition and origin of the Apollo mafic ("LKFM") impact-melt breccias. J. Geophys. Res 105, 4317–4345.

Korotev RL, Gillis JJ, Haskin LA and Jolliff BL (2002) On the age of the Nectaris basin. In The Moon Beyond 2002: Next Steps in Lunar Science and Exploration, #3029 (eds. Lawrence DJ and Duke MB). The Lunar and Planetary Institute, Houston.

Korotev RL, Jolliff BL, Campbell AJ, and Humayun M (2003) Laser-ablation ICP-MS analyses of meteoritic metal grains in lunar impact-melt breccias. Lunar Planet. Sci. XXXIV, #1487 (abstr.).

Krähenbühl U, Ganapathy R, Morgan JW and Anders E (1973) Volatile elements in Apollo 16 samples: Implications for highland volcanism and accretion history of the Moon. *Proc. Lunar Sci. Conf.***4(2),***Geochim. Cosmochim. Acta* (suppl. 4), 1325–1348.

Kring DA and Cohen BA (2002) Cataclysmic bombardment throughout the inner solar system 3.9-4.0 Ga. J. Geophys. Res 107(E2), 4-1 to 4-6.

Lindstrom MM, Marvin UB, Vetter SK and Shervais JW (1988) Apennine front revisited: Diversity of Apollo 15 highland rock types. Proc. Lunar Planet. Sci. Conf 18,169–185.

Lindstrom MM and Salpus PA (1981) Geochemical studies of rocks from North Ray Crater Apollo 16. Proc. Lunar Planet. Sci. Conf 12, 305–322.

Liu D, Jolliff BL, Zeigler RA, Korotev RL, Wan Y, Xie H, Zhang Y, Dong C, and Wang W (2012) Comparative zircon U-Pb geochronology of impact melt breccias from Apollo 12 and lunar meteorite SaU 169, and the age of the Imbrium impact. Earth Planet. Sci. Lett 319-320, 277–286.

Ludwig KR (2003) ISOPLOT 3.00. A geochronological toolkit for Mikrosoft Excel. Berkeley Geochron. Center Spec Publ. 4, 70pp.

Marchi S, Bottke WF, Cohen BA, Wünnemann K, Kring DA, McSween HY, De Sanctis MC, O'Brien DP, Schenk P, Raymond CA, and Russell CT (2013) High-velocity collisions from the lunar cataclysm recorded in asteroidal meteorites. Nature Geosciences 6, 303–307.

Marti K, Aeschlimann U, Eberhardt P, Geiss J, Grögler N, Jost DT, Laul JC, Ma MS, Schmitt RA and Taylor GJ (1983) Pieces of the ancient lunar crust: Ages and composition of clasts in consortium breccia 67915. *Proc. Lunar Planet. Sci. Conf.***14,***J. Geophys. Res.* 88 (Suppl.), B165–B175.

McCoy TJ, Walker RJ, Goldstein JI, Yang J, McDonough WF, Rumble D, Chabot NL, Ash RD, Corrigan CM, Michael JR and Kotula PG (2011) Group IVA irons: New constraints on the crystallization and cooling history of an asteroidal core with a complex history. Geochim. Cosmochim. Acta 75, 6821–6843.

McDonald I, Andreoli MAG, Hart RJ and Tredoux M (2001) Platinum-group elements in the Morokweng impact structure, South Africa: Evidence for the impact of a large ordinary chondrite projectile at the Jurassic-Cretaceous boundary. Geochim. Cosmochim. Acta 65, 299–309.

Mckay DS, Bogard DD, Morris RV, Korotev RL, Johnson P and Wentworth SJ (1986) Apollo 16 regolith breccias: Characterization and evidence for early formation in the megaregolith. *Proc. Lunar Planet. Sci. Conf.***16,***J. Geophys, Res.*,91, D277–D303.

McKinley JP, Taylor GJ, Keil K, Ma M-S and Schmitt RA (1984) Apollo 16: Impact melt sheets, contrasting nature of the Cayley plains and Descartes mountains, and geologic history. *Proc. Lunar Planet. Sci. Conf.***14,***J. Geophys. Res.* 89, B513–B524.

Merle RE, Nemchin AA, Grange ML, Whitehouse MJ and Pidgeon RT (2014) High resolution U-Pb ages of Ca-phosphates in Apollo 14 breccias: Implications for the age of the Imbrium impact. Meteorit. Planet. Sci 49, 2241–2251.

Misra KC and Taylor LA (1975) Characteristics of metal particles in Apollo 16 rocks. Proc. Lunar Sci. Conf 6, 615–639.

Morbidelli A (2010) A coherent and comprehensive model of the evolution of the outer Solar System. Comptes Rendus Physique 11, 651–659.

Morbidelli A, Marchi S, Bottke WF, and Kring DA (2012) A sawtooth-like timeline for the first billion years of lunar bombardment. Earth Planet. Sci. Lett 355-356, 144–151.

Morgan JW, Ganapath R, Higuchi H and Anders E (1974) Lunar, terrestrial, and meteoritic anorthosites - abundances of volatile and siderophile Elements. Transactions-American Geophysical Union 55, 325–326.

Morgan JW, Laul JC, Krähenbühl U, Ganapathy K and Anders E (1972) Major impacts on the Moon: characterization from trace elements in Apollo 12 and 14 samples. *Proc. Lunar Sci. Conf.***3,***Geochim. Cosmochim. Acta*, 2 (Suppl. 3), 1377–1395.

Muehlberger WR, Horz F, Sevier JR and Ulrich GE (1980) Mission objectives for geological exploration of the Apollo 16 landing site. In Proc. Conf. Lunar Highlands Crust, pp. 1–49.

Müller HW, Plieninger T, James OB and Schaeffer OA (1977) Laser probe ^{39}Ar-^{40}Ar dating of materials from consortium breccia 73215. Proc. Lunar Sci. Conf 8, 2551–2565.

Niihara T, and Kring DA (2012a) Petrology of the centimeter-size impact melt clasts in ancient regolith breccia 60016. Lunar Planet. Sci. XXXXIII, #1229 (abstr.).

Niihara T and Kring DA (2012b) Petrology of impact melt clasts in Apollo 16 ancient regolith breccias. 75th Annual Meteoritical Society Meeting, #5074 (abstr.).

Niihara T, Beard SP, Swindle TD, and Kring DA (2013) Evidence for multiple impact events from centimeter-sized impact melt clasts in Apollo 16 ancient regolith breccias: Support for late stage heavy bombardment of the Moon. Lunar Planet. Sci. XXXXIV, #2083 (abstr.).

Norman MD, Bennett VC and Ryder G (2002) Targeting the impactors: siderophile element signatures of lunar impact melts from Serenitatis. Earth Planet. Sci. Lett 202, 217–228.

Norman MD, Duncan RA and Huard JJ (2006) Identifying impact events within the lunar cataclysm from ^{40}Ar-^{39}Ar ages and compositions of Apollo 16 impact melt rocks. Geochim. Cosmochim. Acta 70, 6032–6049.

Norman MD, Duncan RA and Huard JJ (2010) Imbrium provenance for the Apollo 16 Descartes terrain: Argon ages and geochemistry of lunar breccias 67016 and 67455. Geochim. Cosmochim. Acta 74, 763–783.

Norman MD, Shih CY, Nyquist LE, Bogard DD and Taylor LA (2007) Early impacts on the Moon: crystallization ages of Apollo 16 melt breccias. Lunar Planet. Sci. XXXVIII, #1991 (abstr.).

Norman MD and Nemchin AA (2014) A 4.2 billion year old impact basin on the Moon: U—Pb dating of zirconolite and apatite in lunar melt rock 67955. Earth Planet. Sci. Lett 388, 387–398.

Nunes PD, Tatsumoto M, Knight RJ, Unruh DM, and Doe BR (1973) U-Th-Pb systematics of some Apollo 16 lunar samples. Proc. Lunar Sci. Conf 4, 1797–1922.

Nunes PD (1975) Pb loss from Apollo 17 glassy samples and Apollo 16 revisited. Proc. Lunar Sci. Conf 6, 1491–1499.

Papanastassiou DA and Wasserburg GJ (1972) Rb-Sr age of a crystalline rock from Apollo-16. Earth Planet. Sci. Lett 16, 289–298.

Pearson DG, Irvine GJ, Ionov DA, Boyd FR and Dreibus GE (2004) Re-Os isotope systematics and platinum group element fractionation during mantle melt extraction: a study of massif and xenolith peridotite suites. Chem. Geol 208, 29–59.

Pernicka E and Wasson JT (1987) Ru, Re, Os, Pt and Au in iron-meteorites. Geochim. Cosmochim. Acta 51, 1717–1726.

Phinney D, Kahl SB and Reynolds JH (1975) ^{40}Ar-^{39}Ar dating of Apollo 16 and 17 rocks. Proc. Lunar Sci. Conf 6, 1593–1608.

Pidgeon RT, Nemchin AA, vanBronswijk W, Geisler T, Meyer C, Compston W and Williams IS (2007) Complex history of a zircon aggregate from lunar breccia. Geochim. Cosmochim Acta 71, 1370–1381.

Puchtel IS, Walker RJ, James OB and Kring DA (2008) Osmium isotope and highly siderophile element systematics of lunar impact melt breccias: Implications for the late accretion history of the Moon and Earth. Geochim. Cosmochim. Acta 72, 3022–3042.

Rehkämper M and Halliday AN (1997) Development and application of new ion-exchange techniques for the separation of the platinum group and other siderophile elements from geological samples. Talanta 44, 663–672. [PubMed: 18966788]

Reimold WU, Nyquist LE, Bansal BM, Wooden JL, Shih CY, Wiesmann H and Mackinnnon IDR (1985) Isotope analysis of crystalline impact-melt rocks from Apollo 16 stations 11 and 13. North Ray Crater. *Proc. Lunar Planet. Sci. Conf.***15,** J. Geophys. Res. 90, C597–C612.

Rotenberg E, Davis DW, Amelin Y, Ghosh S and Bergquist BA (2012) Determination of the decay-constant of Rb-87 by laboratory accumulation of Sr-87. Geochim. Cosmochim. Acta 85, 41–57.

Ryder G (2002) Mass flux in the ancient Earth-Moon system and benign implications for the origin of life on Earth. J. Geophys. Res. Planet 107 (E4), doi:10.1029/2001JE001583.

Ryder G and Bower JF (1977) Petrology of Apollo 15 black-and-white rocks 15445 and 15455: Fragments of the Imbrium impact melt sheet? Proc. Lunar Sci. Conf 8, 1895–1923.

Ryder G and Norman MD (1980) Catalog of Apollo 16 rocks (3 vol.). Curator's Office pub. #52, JSC #16904.

Ryder G and Wood JA (1977) Serenitatis and Imbrium impact melts: Implications for large-scale layering in the lunar crust. Proc. Lunar Sci. Conf 8, 655–688.

Schultz PH (2001) Origin and implications of the Imbrium sculpture. Lunar Planet. Sci. XXXII Lunar Planet. Inst., Houston. #1900 (abstr.).

Schultz PH, Stickle AM, and Crawford DA (2012) Effect of asteroid decapitation on craters and basins. Lunar Planet. Sci. XLIII Lunar Planet. Inst., Houston. #2428(abstr.).

Sharp M, Gerasimenko I, Loudin LC, Liu J, James OB, Puchtel IS and Walker RJ (2014) Characterization of the dominant impactor signature for Apollo 17 impact melt rocks. Geochim. Cosmochim. Acta 131, 62–80.

Shih CY, Nyquist LE, Dasch EJ, Bogard DD, Bansal BM and Wiesmann H (1993) Ages of pristine noritic clasts from lunar breccia-15445 and breccia-15455. Geochim. Cosmochim. Acta 57, 915–931.

Shirey SB and Walker RJ (1998) The Re-Os isotope system in cosmochemistry and high-temperature geochemistry. Annu. Rev. Earth Pl. Sc 26, 423–500.

Smoliar MI, Walker RJ and Morgan JW (1997) Rhenium-osmium isochron for IA meteorites: Further refinement of the rhenium-187 decay constant. Meteorit. Planet. Sci 32, A122–A123.

Spudis PD and Ryder G (1981) Apollo 17 impact melts and their relation to the Serenitatis basin. Proc. Lunar Planet. Sci. Conf 12, 133–148.

Stöffler D, Bischoff A, Borchardt R, Burghele A, Deutsch A, Jessberger EK, Ostertag R, Palme H, Spettel B, Reimold WU, Wacker K and Wanke H (1985) Composition and evolution of the lunar crust in the Descartes highlands, Apollo-16. J. Geophys. Res 90, C449–C506.

Stöffler D, Ostertag R, Reimold WU and Borchardt R (1981) Stratigraphy and evolution of the upper highland crust near North Ray, Apollo-16. Meteoritics 16, 389–389.

Stöffler D and Ryder G (2001) Stratigraphy and isotope ages of lunar geologic units: Chronological standard for the inner solar system. Space Sci. Rev 96, 9–54.

Stöffler D, Ryder G, Ivanov BA, Artemieva NA, Cintala MJ and Grieve RAF (2006) Cratering history and lunar chronology. New Views of the Moon 60, 519–596.

Strom RG, Maholtra R, Ito T, Yoshida F, and Kring DA, (2005) The origin of planetary impactors in the inner solar system. Science309, 1847–1850. [PubMed: 16166515]

Swann GA, Bailey NG, Batson RM, Eggleton RE, Hait MH, Holt HE, Larson KB, McEwen MC, Mitchell ED, Schaber GG, Schafer JP, Shepard AB, Sutton RL, Trask NJ, Ulrich GE, Wilshire HG and Wolfe EW (1972) 3. Preliminary geologic investigation of the Apollo 14 landing site. In Apollo 14 Preliminary Science Report. NASA SP-272. p. 39–85.

Swann GA, Bailey NG, Batson RM, Eggleton RE, Hait MH, Holt HE, Larson KB, Reed VS, Schaber GG, Sutton RL, Trask NJ, Ulrich GE and Wilshire HG (1977) Geology of the Apollo 14 landing site in the Fra Mauro Highlands. U.S.G.S Prof. Paper 880.

Swindle TD, Beard SP, Isachsen CE, and Kring DA (2012) ^{40}Argon-^{39}Argon ages of centimeter-sized impact melt clasts from ancient regolith breccia 60016. 75th Annual Meteoritical Society Meeting, abstract #5048.

Tera F, Papanastassiou DA and Wasserburg GJ (1974) Isotopic evidence for a terminal lunar cataclysm. Earth Planet. Sci. Lett 22, 1–21.

Turner G, Huneke JC, Podosek FA and Wasserbuerg GJ (1971) ^{40}Ar-^{39}Ar ages and cosmic-ray exposure ages of Apollo-14 samples. Earth Planet. Sci. Lett 12, 19–35.

Turner G and Cadogan PH (1975) The history of lunar bombardment inferred from ^{40}Ar-^{39}Ar dating of highland rocks. Proc. Lunar Sci. Conf 6, 1509–1538.

Ulrich GE (1973) A geologic model for North Ray crater and stratigraphic implications for the Descartes region. *Proc. Lunar Sci. Conf.***4,***Geochim. Cosmochim. Acta*, 1 (Suppl. 4), 27–39.

van Acken D, Brandon AD and Humayun M (2011) High-precision osmium isotopes in enstatite and Rumuruti chondrites. Geochim. Cosmochim. Acta 75, 4020–4036.

Vaniman DT and Papike JJ (1980) Lunar highland melt rocks: Chemistry, petrology and silicate minerology. In Proc. Conf. Lunar Highlands Crust (Papike JJ and Merill RB, eds.), pp. 271–337. Pergamon. Lunar Planetary Institute, Houston.

Walker RJ (2012) Evidence for homogeneous distribution of osmium in the protosolar nebula. Earth Planet. Sci. Lett 351, 36–44.

Walker RJ, Horan MF, Morgan JW, Becker H, Grossman JN and Rubin AE (2002) Comparative ^{187}Re-^{187}Os systematics of chondrites: Implications regarding early solar system processes. Geochim. Cosmochim. Acta 66, 4187–4201.

Walker RJ, McDonough WF, Honesto J, Chabot NL, Mccoy TJ, Ash RD and Bellucci JJ (2008) Modeling fractional crystallization of group IVB iron meteorites. Geochim. Cosmochim. Acta 72, 2198–2216.

Walsh KJ, Morbidelli A, Raymond SN, O'Brien DP and Mandell AM (2011) A low mass for Mars from Jupiter's early gas-driven migration. Nature 475, 206–209. [PubMed: 21642961]

Wänke H, Palme H, Kruse H, Baddenhausen H, Cendales M, Dreibus G, Hofmeister H, Jagoutz E, Palme C, Spettel B and Thacker R (1976) Chemistry of lunar highland rocks: a refined evaluation of the composition of the primary matter. Proc. Lunar Sci. Conf 7, 3479–3499.

Warner JL, Simonds CH and Phinney WC (1973) Apollo 16 rocks: Classification and petrogenetic model. Proc. Lunar Sci. Conf 4, 481–504.

Warner RD, Dowty E, Prinz M, Conrad GH, Nehru CE and Keil K (1976) Catalog of Apollo 16 rake samples from the LM area and station 5. Spec. Publ #13, UNM Institute of Meteoritics, Albuquerque, 87pp.

Warren PH and Wasson JT (1978) Compositional petrographic investigation of pristine nonmare rocks. Proc. Lunar Planet. Sci. Conf 9, 185–217.

Warren PH and Wasson JT (1979) The compositionalpetrographic search for pristine nonmare rocks: Third foray. Proc. Lunar Planet. Sci. Conf 10, 583–610.

Warren PH and Wasson JT (1980) Further foraging of pristine nonmare rocks: Correlations between geochemistry and longitude. Proc. Lunar Planet. Sci. Conf 11, 431–470.

Wasson JT (1999) Trapped melt in IIIAB irons; solid/liquid elemental partitioning during the fractionation of the IIIAB magma. Geochim. Cosmochim. Acta 63, 2875–2889.

Wasson JT, Boynton WV, Chou CL and Baedecker PA (1975) Compositional evidence regarding influx of interplanetary materials onto lunar-surface. Moon 13, 121–141.

Wasson JT, Huber H and Malvin DJ (2007) Formation of IIAB iron meteorites. Geochim. Cosmochim. Acta 71, 760–781.

Wasson JT and Richardson JW (2001) Fractionation trends among IVA iron meteorites: Contrasts with IIIAB trends. Geochim. Cosmochim. Acta 65, 951–970.

Wasson JT, Warren PH, Kallemeyn GW, McEwing CE, Mittlefehldt DW and Boynton WV (1977) SCCRV, a major component of highlands rocks. Proc. Lunar Sci. Conf 8, 2237–2252.

Wieczorek MA, Weiss BP, and Stewart ST (2012) An impactor origin for lunar magnetic anomalies. Science 335, 1212–1215. [PubMed: 22403388]

Wilhelms DE (1972) Reinterpretation of the northern Nectaris basin. *Apollo 16 Preliminary Science Report*, NASA SP-315, 29–27 to 29–30.

Wilshire HG and Jackson ED (1972) Petrology and stratigraphy of the Fra Mauro Formation at the Apollo 14 site. U.S. Geol. Survey Prof Paper 785.

York D, Kenyon WJ and Doyle RJ (1972) 40Ar-39Ar ages of Apollo 14 and 15 samples. Proc. Lunar Sci. Conf 3, 1613–1622.

Yang J, Goldstein JI, and Scott ERD (2007) Iron meteorite evidence for early formation and catastrophic disruption of protoplanets. Nature 446, 888–891. [PubMed: 17443181]

Yang J, Goldstein JI, and Scott ERD (2008) Metallographic cooling rates and origin of IVA iron meteorites. Geochim. Cosmochim. Acta 72, 3043–3061.

Zipfel J, Spettel B, Palme H, Wolf D, Franchi I, Sexton AS, Pillinger CT and Bischoff A (1998) Dar al Gani 400: chemistry and petrology of the largest lunar meteorite. Meteorit. Planet. Sci 33, A171 (abstr.).

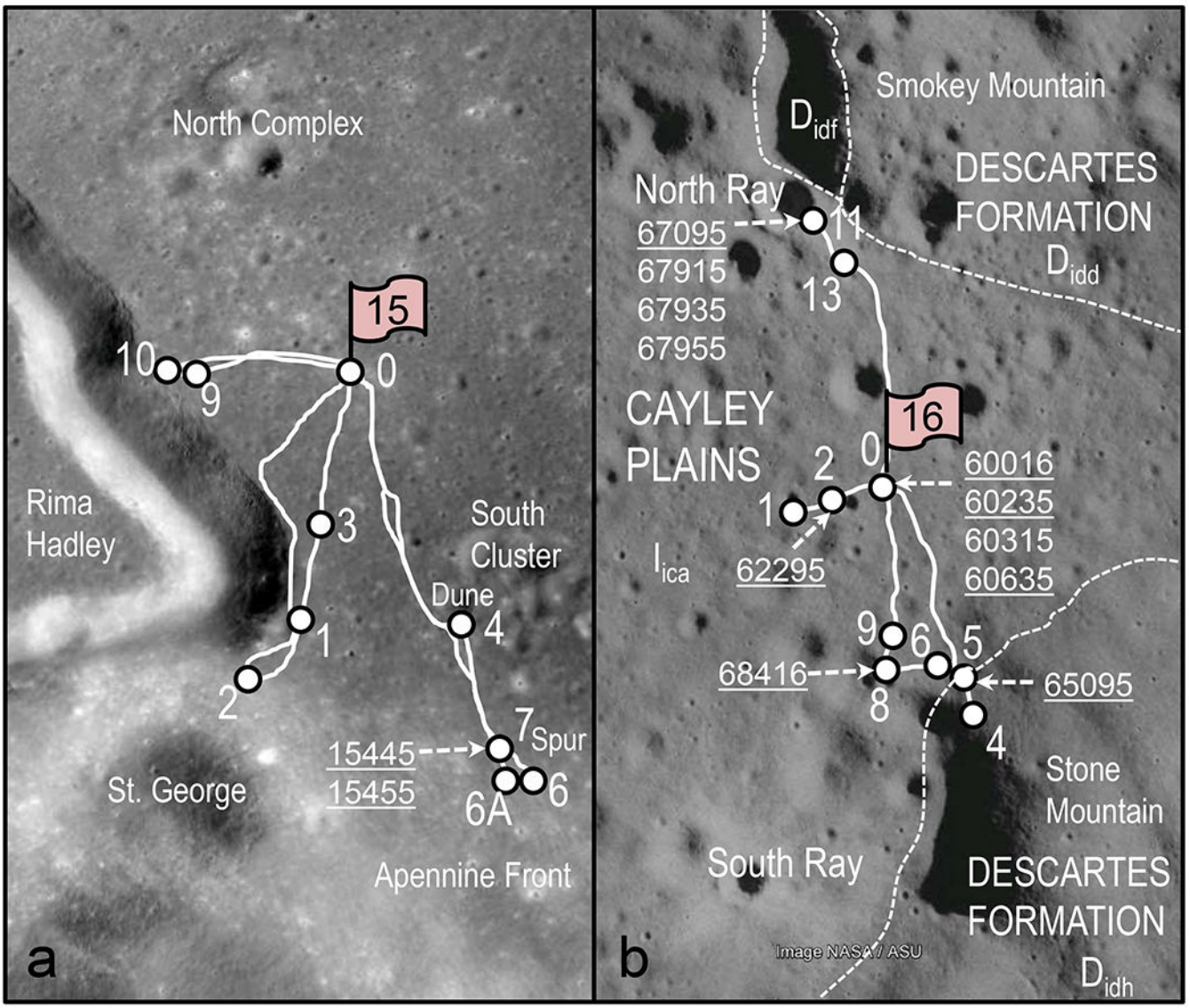

Fig. 1.

Apollo 15 (**a**) and 16 (**b**) mission traverse route and sample stations with collection locations of the impact melt rock samples that have been determined for the HSE concentrations and Os isotopic compositions. Underlined sample numbers denote samples examined in this study. Data are overlain on Apollo metric camera mosaic (NASA/ASU) in Google Moon. For the Apollo 16 site, geological boundary between the Cayley Plains Formation and Descartes Formation (Hodges, 1972) is denoted using white dashes. Stone Mountain to the south is part of the Descartes hilly unit D_{idh}. Smoky Mountain to the north is part of the Descartes domed unit D_{idd} with a small furrowed unit D_{idf}.

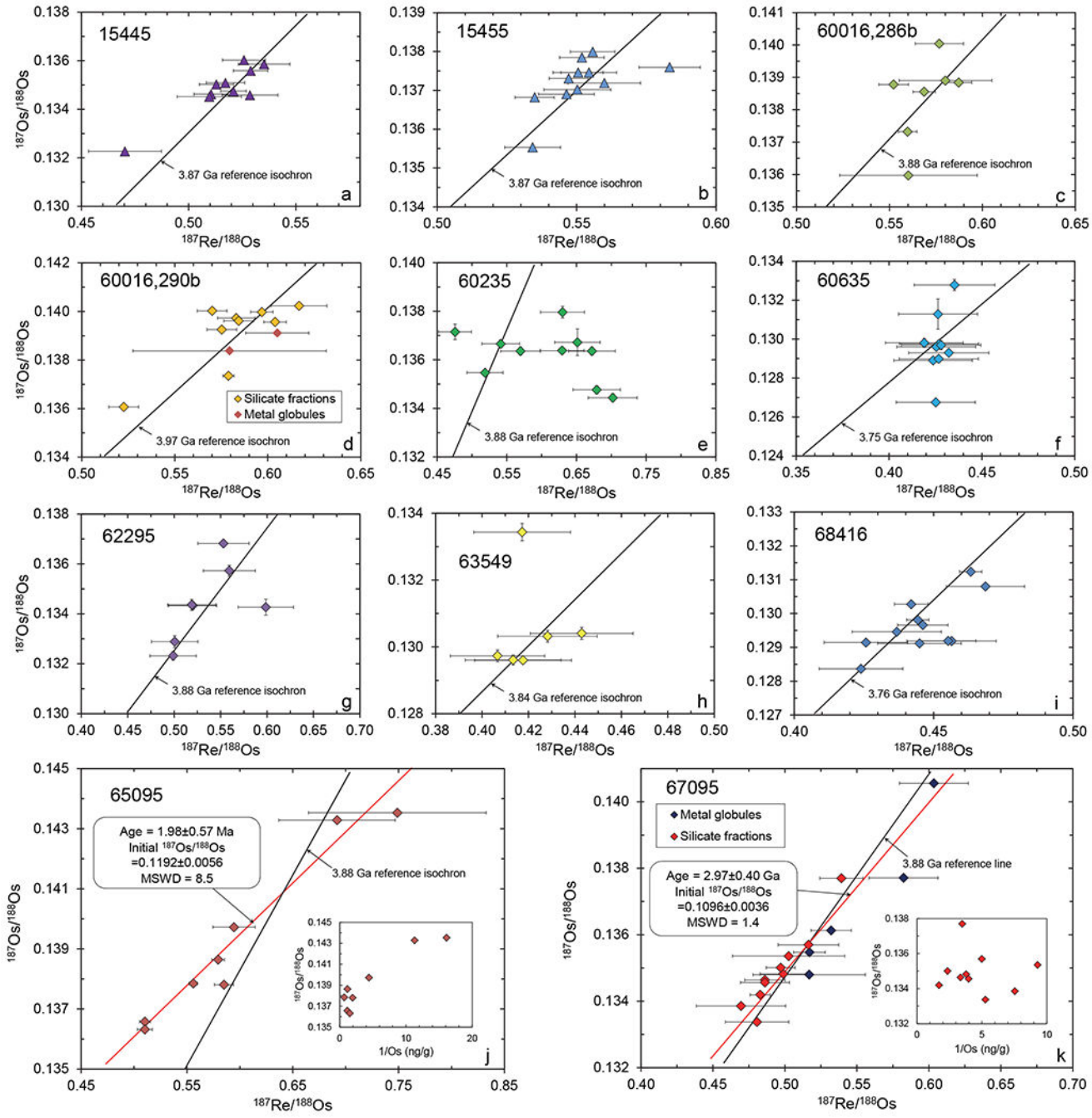

Fig. 2a-k.

$^{187}Os/^{188}Os$ and $^{187}Re/^{188}Os$ isotope systematics for subsamples of the 11 Apollo 15 and 16 lunar impact melt rocks. Errors (2**σ**) are as provided in Table 2. No robust isochrons are observed. The black line in each panel denotes a reference isochron that is appropriate for the reported age of the rock. For samples 65095 (**j**) and 67095 (**k**) the plots include data for both bulk silicate fractions and individual metal grains as 60016,290b. The red line is the regression of the data and the inset shows the correlation for $^{187}Os/^{188}Os$ versus 1/Os for subsamples.

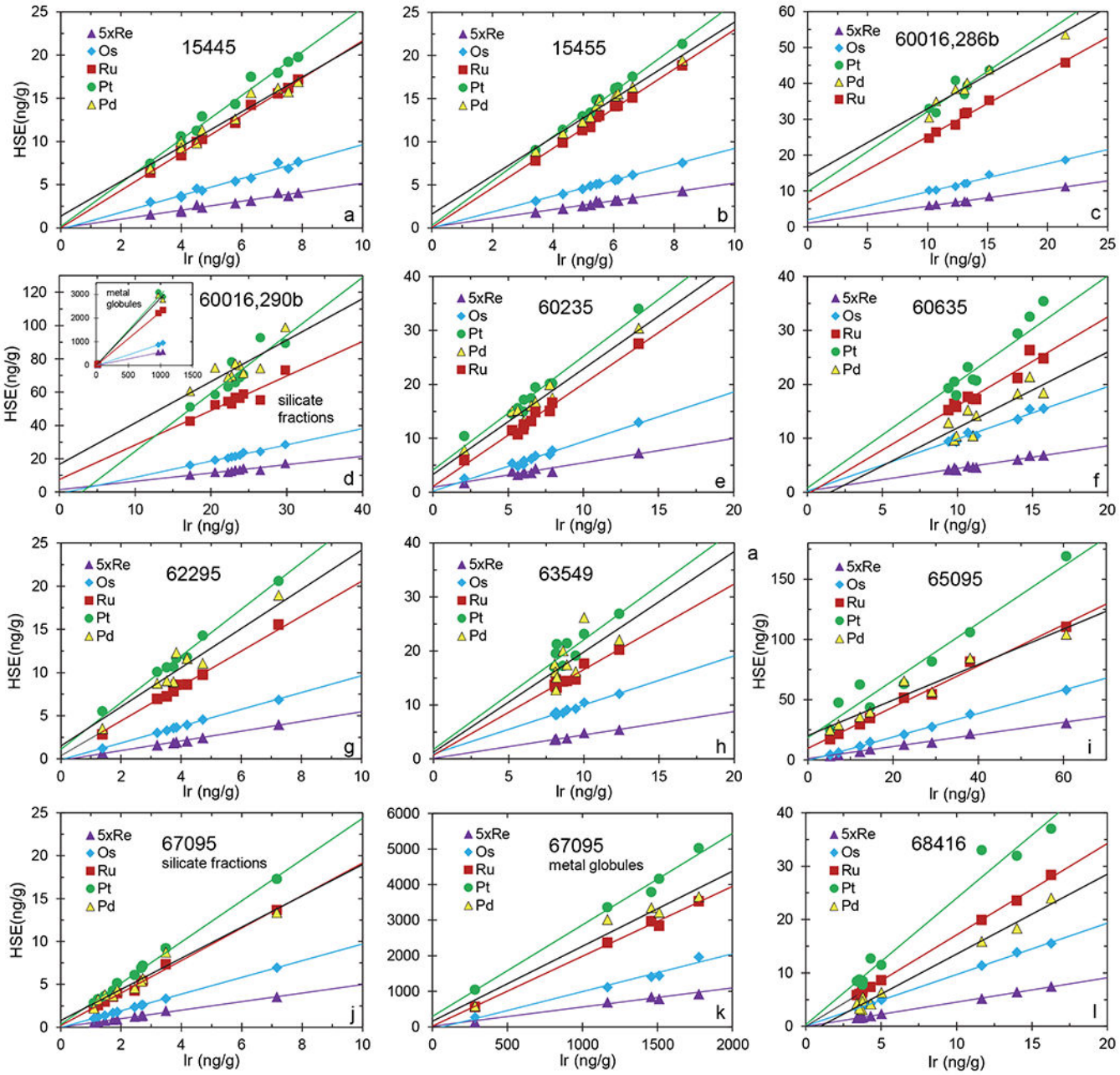

Fig. 3.

Linear regressions of HSE versus Ir concentrations for the eleven Apollo 15 and 16 lunar impact melt rocks. The subsamples for most melt rocks form well-defined linear trends with near-zero y-intercepts resulting from contamination of a single dominant impactor, while the subsamples for some rocks (e.g., lithic clasts from regolith breccias) form more scattered trends with non-zero intercepts resulting from contamination of multiple impactor components. Details about the interpretation for scattered trends and non-zero y-intercepts, as well as the determination of the HSE characteristics of the impactors involved, are provided in the text.

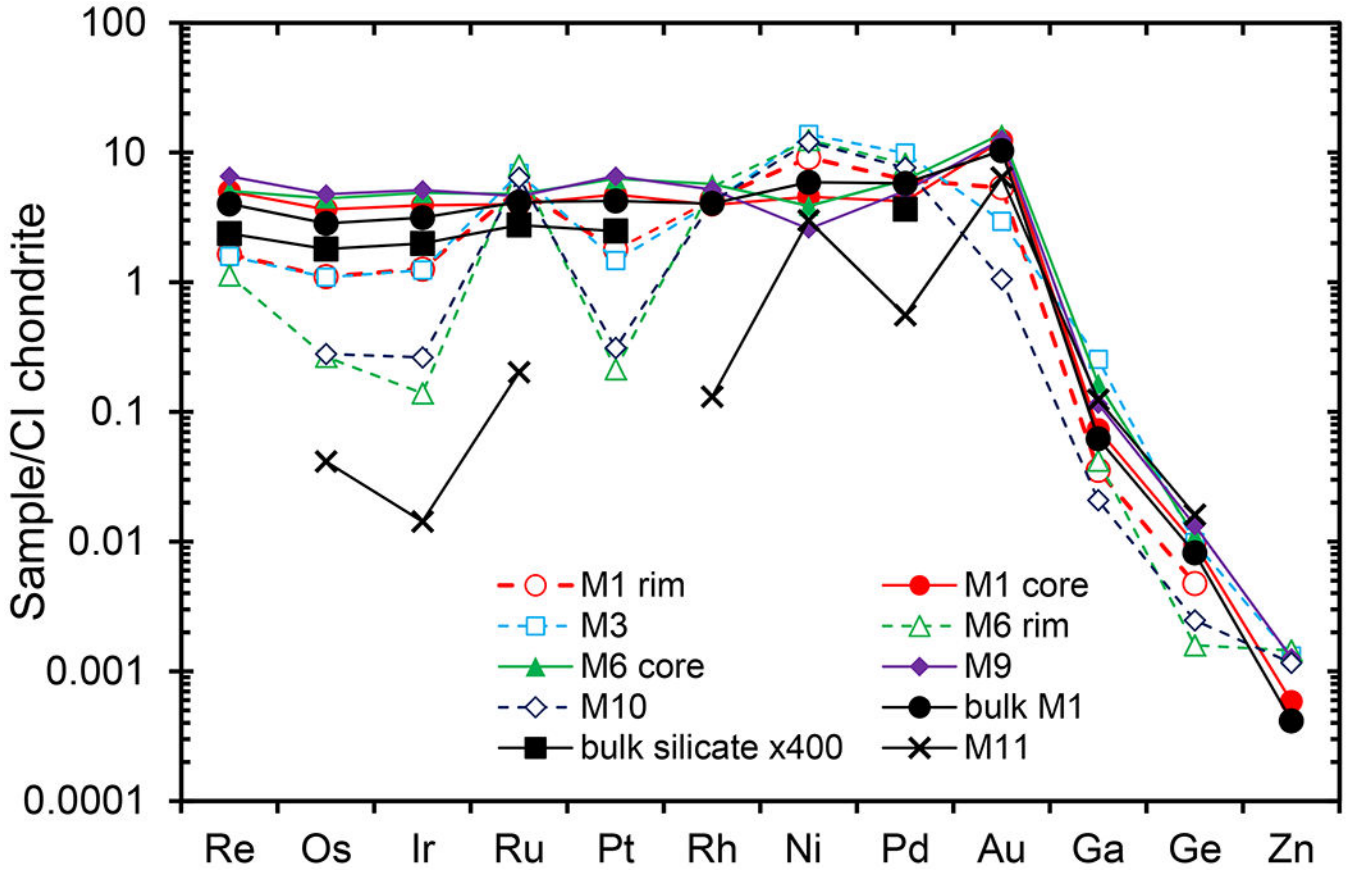

Fig. 4.

CI chondrite normalized patterns of siderophile element data for the 67095 metal grains obtained by *in situ* laser ablation ICP-MS analysis. The elements are arranged in order such that the 50% condensation temperatures decrease from left to right. The bulk silicate rock composition, multiplied by 400, of 67095 was determined by isotope dilution (data in Table 2) is plotted for comparison. CI values are from Horan et al. (2003) and Fischer-Gödde et al. (2010). Calculations show that the bulk HSE composition of grain M1 can be accounted for assuming a rim thickness of approximately one tenth of the grain radius with a mass proportion of roughly 3:7; using this mass proportion, the rest of siderophile elements are calculated and shown in the Electronic Annex.

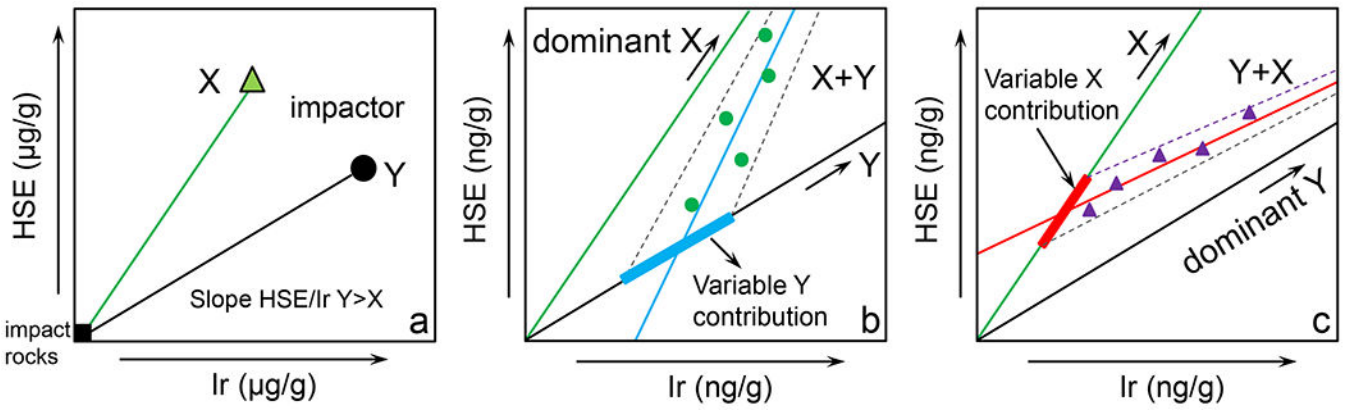

Fig. 5.

Schematic illustration of the mixing HSE versus Ir trends between the HSE-rich impactor(s) and the HSE-free lunar pristine rocks. For a given impact melt rock with linear trends and zero y-intercepts, this indicates contamination of a single dominant impactor as shown by the green (X) or black (Y) line in each panel; here (**a**) it is assumed that HSE/Ir ratios of X are greater than those of Y. In this case, the averaged $^{187}Os/^{188}Os$ and regressed HSE/Ir ratios can be used to precisely estimate the relative composition of the meteoritic impactor X or Y. For one impact rock with scattered trends and non-zero y-intercepts, this indicates incorporation of multiple impactor impactors. Assuming that there are two impactors X and Y, if X, compared to Y, imparts the greater proportion of HSE into the impact melt, this would lead to the creation of HSE versus Ir trends with scatter primarily controlled by the variable HSE contribution from Y, as well as negative y-intercepts (**b**). If Y is the dominant impactor imparting the greater proportion of HSE, this would cause HSE versus Ir trends with scatter and positive y-intercepts (**c**). It should be noted that efficient homogenization of multiple impactor components into melt rocks can possibly generate linear HSE versus Ir trends with zero y-intercepts as a single impactor (Fischer-Gödde and Becker, 2012). More details are provided in the text.

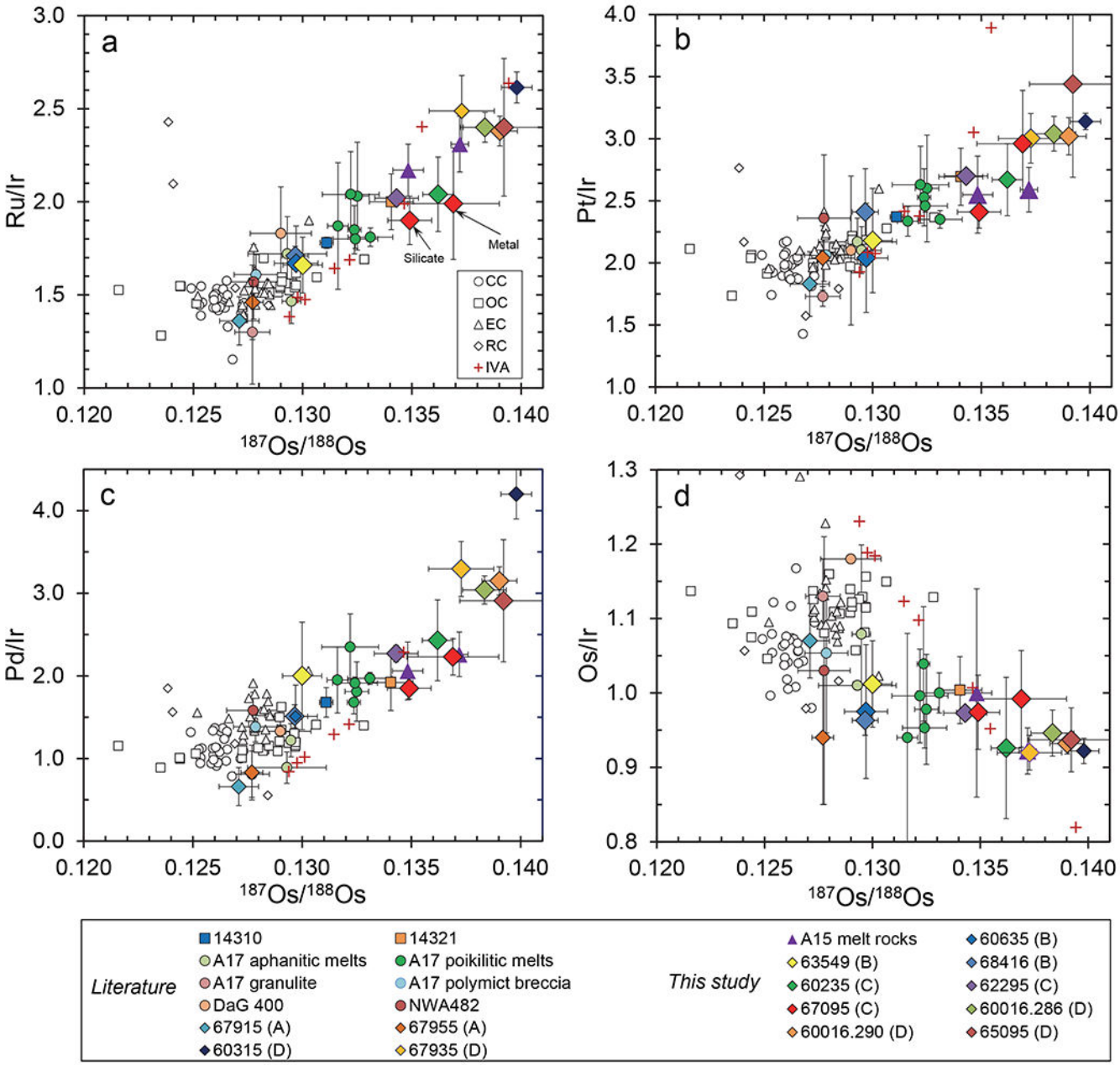

Fig. 6.

Average $^{187}Os/^{188}Os$ versus regressed or averaged Ru/Ir (**a**), Pt/Ir (**b**), Pd/Ir (**c**), and Os/Ir (**d**) for the impactor components present in the lunar impact melt rocks examined here and in the literature in comparison with ratios of chondrites, and IVA iron meteorites. Errors for $^{187}Os/^{188}Os$ of the impactor component are expressed as $2\sigma_{mean}$ (Table 2), while errors for elemental ratios either reflect 2σ uncertainties from the regression calculations (regressed ratios for a single impactor component) or are shown as $2\sigma_{mean}$ from the simple ratio calculations (averaged ratios for the multiple impactor components; data in Table 3). Based on the HSE signature discussed in the text, the Apollo 16 melt rocks are divided into four groups (A, B, C and D) that are marked in the parentheses after the sample names in the

legend. Data sources for chondrites are from Walker et al. (2002), Horan et al. (2003), Brandon et al. (2005a,b), and Fischer-Gödde et al. (2010), and for IVA iron meteorites are from McCoy et al. (2011). Literature data of lunar impact melt rocks are from Norman et al. (2002), Puchtel et al. (2008), Fischer-Gödde and Becker (2012), and Sharp et al. (2014).

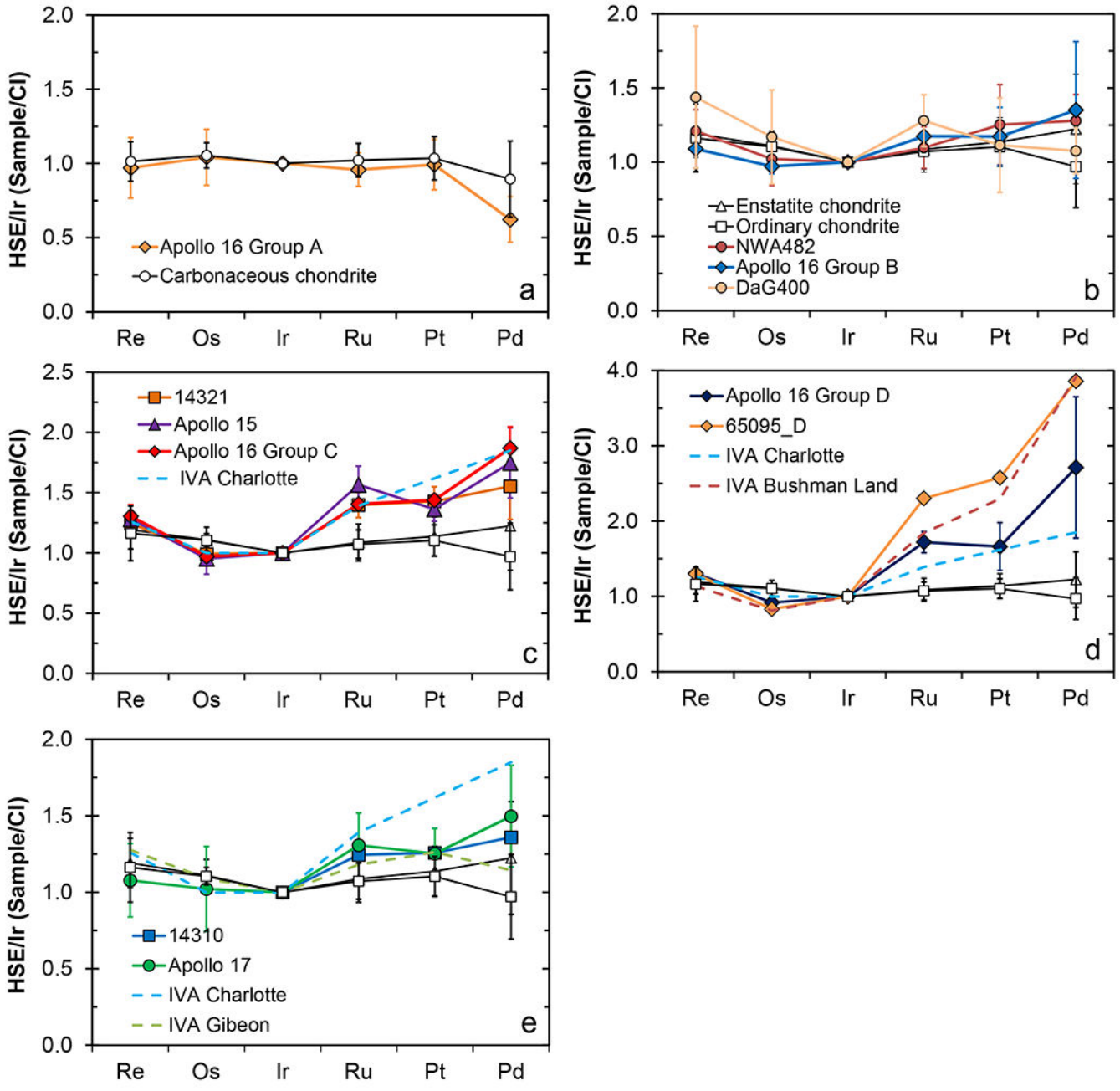

Fig. 7.

Double normalized HSE concentration patterns (normalized to Ir and CI chondrite values) for all the lunar impact melt rocks (Table 5, this study, Norman et al., 2002; Puchtel et al., 2008; Fischer-Gödde and Becker, 2012; Sharp et al., 2014) that have high-precision HSE data. The average HSE compositions of carbonaceous, enstatite and ordinary chondrites, and selected members of the IVA iron meteorite group are shown for comparison. Data sources for chondrites from Walker et al. (2002), Horan et al. (2003), Fischer-Gödde et al. (2010) and IVA iron meteorites from McCoy et al. (2011).

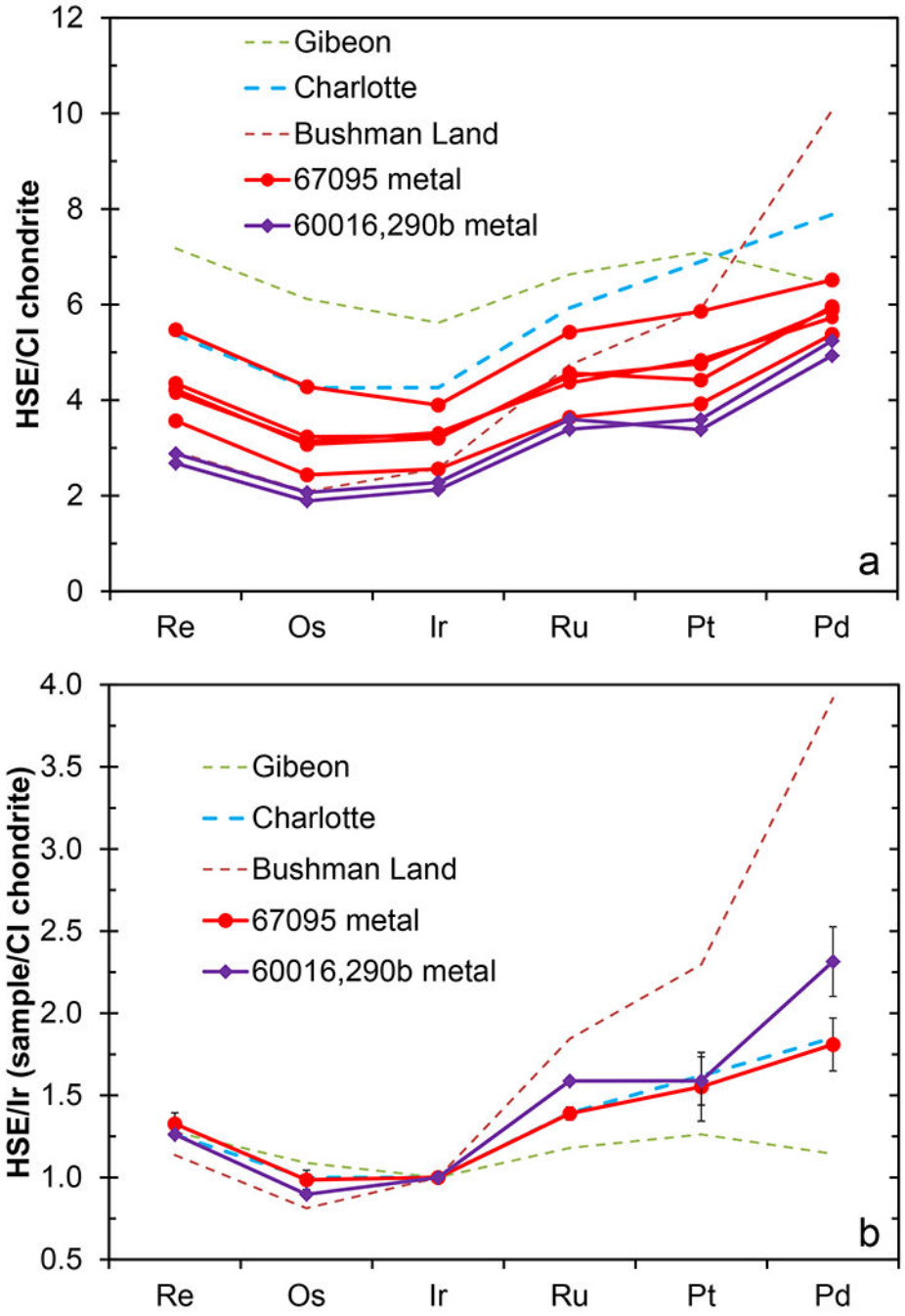

Fig. 8.

a. CI-chondrite normalized HSE patterns for the bulk individual metal grains from 67095 and 60016,290b. **b**. Double normalized HSE concentration patterns for the average compositions of the bulk metals from these two samples. Also shown are selected members (i.e., Bushman Land, Charlotte, and Gibeon) of the IVA iron group (McCoy et al., 2011). CI values are from Horan et al. (2003) and Fischer-Gödde et al. (2010).

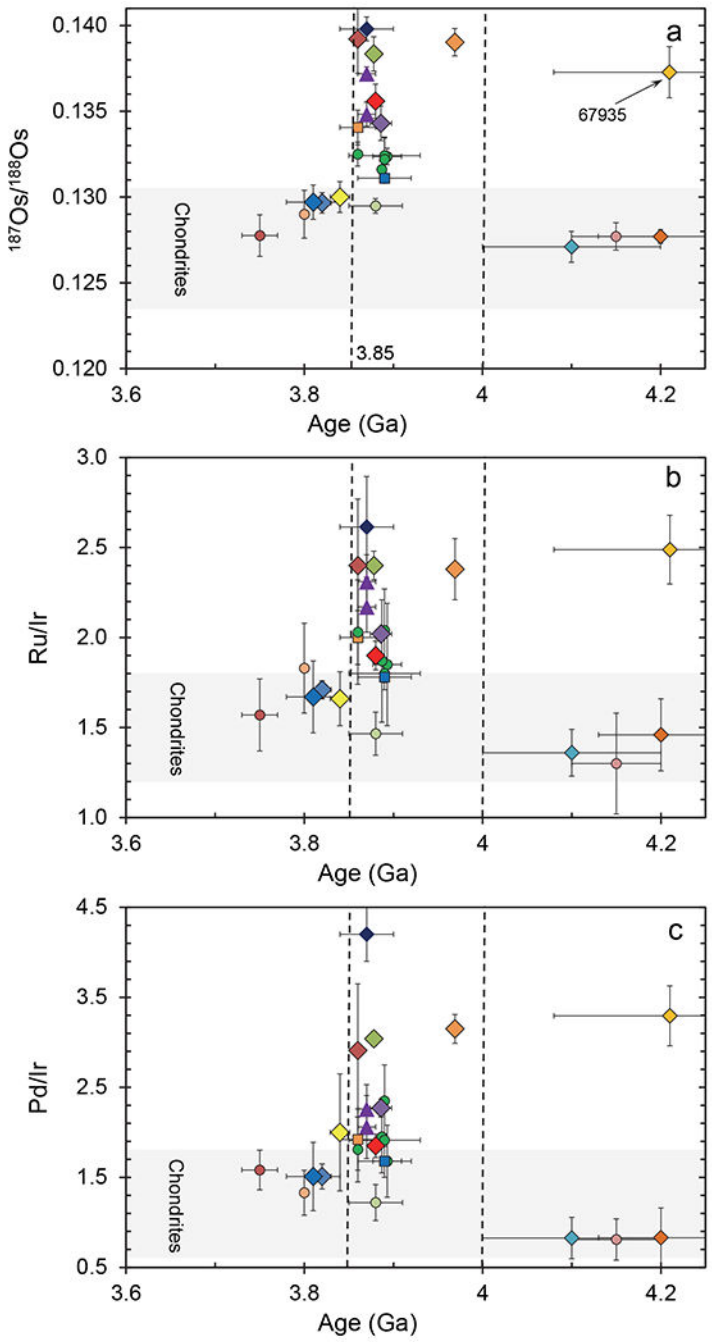

Fig. 9.

Regressed or averaged $^{187}Os/^{188}Os$ (**a**), Ru/Ir (**b**) and Pd/Ir (**c**) versus formation ages (listed in Table 1) for the lunar impact melt rocks examined here and in literature. Vertical dashed lines denote the period of large-basin formation during the putative late heavy bombardment with Imbrium and Serenitatis events highlighted. Horizontal field represents the range of known chondrite groups. Symbols and data sources are the same as Fig. 6.

Table 1.

Petrological and geochronological summary of lunar impact melt rocks that have been determined for highly siderophile element concentrations and Os isotopic compositions using the isotope dilution technique

Sample	Rock type	Ar-Ar plateau age, unless otherwise stated	subsample for HSE measurement
Apollo 14			
14310	impact melt	3.89-3.92 Ga (Turner et al., 1971; Schaeffer and Schaeffer, 1977); Rb-Sr: 3.87 Ga (Papanastassiou and Wasserburg, 1971)	14310,35 (Fischer-Gödde and Becker, 2012)
14321	melt breccia	≤3.86 Ga (York et al., 1972)	14321,1770 (Puchtel et al., 2008)
Apollo 15			
15445	melt breccia	3.76 ± 0.09 Ga? (Bernstein, 1983; no flat plateau)	15445,299 (this study)
15455	melt breccia	3.82-3.94 Ga (Shih et al., 1993; Alexander and Kahl, 1974)	15455,326 (this study)
Apollo 16			
60016	regolith breccia	cosolidated at ~3.74 Ga (Joy et al., 2011); clasts: ,286 (3.878 ± 0.014 Ma) and ,290 (3.969 ± 0.012 Ga) (Niihara et al., 2013)	Clasts 60016,286b & 290b (this study)
60235	melt breccia	No age reported	60235,11 (this study)
60315	impact melt	3.87 ± 0.03 Ga (Norman et al., 2006); Pb-Pb: 3.93-3.99 Ga (Nunes et al., 1973; Nunes, 1975)	60315,46 (Fischer-Gödde and Becker, 2012)
60635	impact melt	two Rb-Sr ages: 3.93 ± 0.02 Ga for coarse-grained portion, and 3.81 ± 0.03 Ga for fine-grained portion (Deutsch and Stoffler, 1987)	60635,18 (this study)
62295	melt breccia	3.886 ± 0.012 Ga (Norman et al., 2006)	62295,188 (this study)
63549	impact melt	3.840 ± 0.011 Ga (Norman et al., 2006)	63549,33 (this study)
65095	regolith breccia	Clast , 118 (3.884 ± 0.017 Ga; Niihara et al., 2013)	Clast 65095,106b (this study)
67095	impact melt	3.879 ± 0.022 Ga (67095,124; Fagan et al., 2013)	67095,125 (this study)
68416	impact melt	Rb-Sr: 3.82 ± 0.01 Ga (Papanastassiou and Wasserburg, 1972; Reimold et al., 1985)	68416,16 (this study)
67915	polymict breccia	3.9 to 4.3 Ga (Kirsten et al., 1973; Marti et al. 1983)	67915,322 (Fischer-Gödde and Becker, 2012)
67935	impact melt	Re-Os: 4.21 ± 0.13 Ga (Fischer-Godde and Becker, 2012), however excluding the lowest ratio, it yields 3.74±0.42 Ga within the range of 3.8 and 4.0 Ga.	67935,29 (Fischer-Gödde and Becker, 2012)
67955	granulite	Sm-Nd: 4.20 ± 0.07 Ga (Norman et al., 2007)	67955,87 (Fischer-Gödde and Becker, 2012)
Apollo 17			
72395	poikilitic breccia	3.893 ± 0.016 Ga (Dalrymple and Ryder,1996)	72395,52 (Puchtel et al., 2008)
72435	micropoikilitic melt breccia	3.86 ± 0.07 Ga (Huneke et al., 1977); Rb-Sr: 3.85 ± 0.18 Ga (Papanastassiou and Wasserburg, 1975)	72435,85 (Sharp et al., 2014)
72535	melt breccia	3.887 ± 0.016 Ga (Dalrymple and Ryder, 1996)	72535,22 (Sharp et al., 2014)
73215	aphanitic breccia	~3.87 Ga (Müller et al., 1977; Jessberger et al., 1978); Rb-Sr: ≤3.90 ± 0.05 Ga (Compston et al., 1977)	73215,643 (Puchtel et al., 2008)
73235	aphanitic melt breccia	3.91 ± 0.04 Ga (Cadogan and Turner, 1975; Phinney et al. 1975); U-Pb of zircon: 4.1-4.4 Ga (Pidgeon et al. 2007)	73235,14 (Sharp et al., 2014)
73255	aphanitic breccia	3.88 ± 0.03 Ga (Jessberger et al., 1978)	73255,623 (Puchtel et al., 2008)
76035	melt breccia	No age reported	76035,35 (Sharp et al., 2014)
76055	polymict breccia	3.93-4.0 Ga (Huneke et al. 1973; Kirsten et al. 1973; Kirsten and Horn 1974); Rb-Sr: 3.86 ± 0.04 Ga (Turner et al. 1973)	76055,93 (Sharp et al., 2014)
76135	poikilitic breccia	No age reported	76215,39 (Sharp et al., 2014)
76215	poikilitic breccia	3.89 ± 0.04 Ga (Cadogan and Turner, 1976)	76215,47 (Puchtel et al., 2008)

Sample	Rock type	Ar-Ar plateau age, unless otherwise stated	subsample for HSE measurement
79215	granulite	4.15 ± 0.05 Ga (Hudgins et al., 2008)	79215,129 (Fischer-Gödde and Becker, 2012)
Lunar meteorites			
DaG 400	regolith breccia	<3.8 Ga (Cohen et al., 2005)	MPI 1292/2 (Fischer-Gödde and Becker, 2012)
NWA 482	melt breccia	~3.75 Ga (Daubar et al., 2002)	Puchtel et al., 2008

Note: all ages are recalculated using latest decay constants.

Table 2.

Highly siderophile element concentrations (ng/g), $^{187}Os/^{188}Os$ and $^{187}Re/^{188}Os$ data of Apollo 15 and 16 impact melt rocks

Sample	Wt. (g)	Re_{meas}	Re*calc[a]	Os	Ir	Ru	Pt	Pd	$^{187}Os/^{188}Os \pm 2\sigma$[b]		$^{187}Re/^{188}Os_{meas} \pm 2\sigma$[b]		$^{187}Re/^{188}Os_{calc}$
Apollo 15 impact melt breccia 15445,299 (10 subsamples, totaling ~0.90 g)													
15445_A1	0.1113	0.740	0.724	6.848	7.55	16.2	19.2	15.7	0.13475	±6	0.521	±6	0.500
15445_B1	0.1049	0.410	0.402	3.698	3.99	8.98	10.6	10.0	0.13586	±6	0.535	±12	0.514
15445_C1	0.0946	0.569	0.567	5.378	5.79	12.1	14.3	12.6	0.13462	±6	0.511	±8	0.498
15445_D1	0.1091	0.472	0.472	4.327	4.69	10.3	12.9	11.3	0.13603	±6	0.526	±10	0.516
15445_F1	0.0896	0.631	0.622	5.758	6.31	14.2	17.5	15.6	0.13559	±7	0.529	±8	0.510
15445_A2	0.0984	0.310	0.312	2.971	2.98	6.35	7.40	6.90	0.13452	±8	0.510	±15	0.497
15445_B2	0.0738	0.345	0.350	3.536	4.00	8.40	9.79	9.27	0.13227	±7	0.470	±17	0.468
15445_B3	0.0679	0.810	0.805	7.549	7.20	15.6	17.9	16.2	0.13509	±8	0.517	±9	0.504
15445_D2	0.0802	0.497	0.477	4.534	4.51	9.93	11.23	9.82	0.13458	±5	0.529	±13	0.498
15445_F2	0.0744	0.813	0.814	7.645	7.88	17.1	19.8	16.9	0.13503	±6	0.513	±8	0.503
Average[c]		0.56	0.55	5.14	5.43	11.8	13.9	12.3	0.1348	±7	0.524	±11	0.501
Apollo 15 impact melt breccia 15455,326 (11 subsamples, totaling ~1.06 g)													
15455_A2	0.1152	0.362	0.351	3.122	3.43	7.82	9.04	8.93	0.13719	±7	0.560	±13	0.531
15455_A3a	0.0988	0.513	0.505	4.530	4.97	11.3	12.9	12.3	0.13690	±6	0.546	±10	0.527
15455_B1a	0.0992	0.645	0.643	5.638	6.06	14.1	16.2	15.3	0.13785	±6	0.552	±8	0.539
15455_B2a	0.1035	0.682	0.684	6.146	6.62	15.1	17.5	16.3	0.13682	±7	0.535	±7	0.526
15455_C1	0.0986	0.638	0.634	5.541	6.05	14.3	16.0	15.3	0.13799	±6	0.556	±8	0.541
15455_A3b	0.0889	0.612	0.574	5.064	5.43	12.9	14.8	14.2	0.13759	±5	0.583	±11	0.536
15455_A3c	0.0965	0.539	0.525	4.870	5.23	11.7	13.4	12.9	0.13553	±5	0.534	±10	0.510
15455_B1b	0.0897	0.856	0.850	7.551	8.27	18.9	21.3	19.5	0.13731	±5	0.547	±7	0.532
15455_B2b	0.0877	0.642	0.636	5.625	6.14	14.2	16.3	15.6	0.13746	±6	0.551	±9	0.534
15455_B1c	0.0953	0.449	0.440	3.935	4.33	9.9	11.4	11.0	0.13702	±6	0.550	±12	0.529
15455_C2	0.0882	0.590	0.580	5.134	5.53	13.1	14.9	14.8	0.13746	±5	0.554	±10	0.534
Average		0.59	0.58	5.15	5.59	12.9	14.8	14.1	0.1372	±4	0.553	±10	0.531
Apollo 16 ancient regolith breccia Clast 60016,286b (7 silicate subsmaples, totaling ~0.291 g)													
,286b_A1	0.0603	1.370	1.313	11.25	12.3	28.4	40.8	38.3	0.13884	±7	0.587	±7	0.552
,286b_B1	0.0591	1.421	1.397	12.05	13.0	31.6	36.9	38.2	0.13856	±8	0.569	±6	0.548
,286b_C1	0.0492	1.385	1.411	12.10	13.3	31.9	39.3	40.2	0.13878	±6	0.552	±8	0.551
,286b_D1	0.0743	1.687	1.638	14.54	15.1	35.3	43.6	43.9	0.13732	±7	0.560	±5	0.532
,286b_A2	0.0178	1.230	1.195	10.23	10.7	26.4	31.8	35.0	0.13890	±6	0.580	±25	0.552
,286b_A3	0.0124	1.180	1.108	10.16	10.1	24.7	33.0	30.4	0.13597	±9	0.560	±37	0.515
,286b_C2	0.0181	2.229	2.236	18.65	21.5	45.8	116	53.5	0.14004	±7	0.577	±13	0.567
Average		1.50	1.47	12.75	13.7	32.2	44.3	40.4	0.1383	±10	0.569	±10	0.545
Apollo 16 ancient regolith breccia Clast 60016,290b (9 silicate subsmaples and 2 metal globules, totaling ~0.286 g)													

Sample	Wt. (g)	Re_{meas}	$Re^{*}calc^{a}$	Os	Ir	Ru	Pt	Pd	$^{187}Os/^{188}Os \pm 2\sigma^{b}$		$^{187}Re/^{188}Os_{meas} \pm 2\sigma^{b}$		$^{187}Re/^{188}Os_{calc}$
,290b_A1b	0.0218	2.633	2.656	24.30	26.5	55.4	92.7	74.4	0.13607	±8	0.523	±8	0.516
,290b_A1c	0.0193	2.677	2.638	22.16	23.8	56.5	68.7	76.2	0.13973	±7	0.583	±10	0.563
,290b_B1b	0.0279	2.510	2.481	21.05	22.7	53.0	78.2	69.9	0.13926	±7	0.575	±8	0.557
,290b_B1c	0.0294	2.415	2.451	20.44	22.2	54.6	63.2	69.2	0.14003	±9	0.570	±8	0.567
,290b_B2b	0.0189	2.075	1.955	16.24	17.2	42.8	51.3	60.7	0.14023	±8	0.617	±15	0.569
,290b_B2c	0.0200	3.466	3.399	28.62	29.8	73.3	89.5	99.0	0.13962	±8	0.584	±8	0.561
,290b_A1	0.0653	2.862	2.688	23.85	24.3	58.9	70.7	71.4	0.13735	±8	0.579	±3	0.533
,290b_B1a	0.0405	2.662	2.578	21.53	23.2	57.0	65.8	77.2	0.13998	±8	0.597	±6	0.566
,290b_B2a	0.0423	2.407	2.282	19.23	20.5	52.6	58.7	74.7	0.13957	±7	0.604	±6	0.561
Metals													
,290b_M1	0.000320	109	102	868	969	2209	3087	2950	0.13911	±11	0.605	±17	0.555
,290b_M2	0.000091	114	110	948	1038	2345	2901	2775	0.13838	±8	0.579	±52	0.546
Average		2.80	2.71	23.20	24.6	59.3	74.0	78.2	0.1390	±8	0.583	±15	0.554
Apollo 16 impact melt 60235,11 (10 silicate subsamples, totalling ~1.16 g)													
60235_A1	0.1423	0.721	0.569	5.167	6.00	11.67	14.97	13.23	0.13636	±16	0.672		0.521
60235_A2	0.1321	0.778	0.560	5.343	5.26	11.44	14.53	15.04	0.13444	±16	0.702		0.497
60235_B1	0.1514	1.456	1.436	12.96	13.68	27.52	34.02	30.47	0.13666	±16	0.541		0.525
60235_B2	0.0593	0.653	0.536	4.829	5.64	10.72	15.59	15.21	0.13672	±55	0.651		0.526
60235_C1	0.1032	0.356	0.267	2.525	2.07	5.91	10.43	7.89	0.13477	±16	0.679		0.501
60235_C2	0.0825	0.732	0.681	6.191	6.52	13.17	17.40	16.08	0.13636	±16	0.570		0.521
60235_D1	0.1003	0.764	0.668	5.846	6.04	12.53	17.15	13.23	0.13796	±24	0.630		0.541
60235_D2	0.1426	0.766	0.870	7.760	7.94	16.56	20.17	17.53	0.13715	±32	0.476		0.531
60235_E	0.1152	n.d.	0.754	7.001	7.76	15.08	20.11	19.96	0.13547	±12	1.112		0.510
60235_F	0.1277	0.887	0.747	6.788	6.81	14.84	19.43	16.79	0.13638	±10	0.629		0.521
average		0.744	0.745	6.768	7.10	14.63	19.05	17.12	0.1362	±10	0.645		0.519
Apollo 16 impact melt 60635,18 (10 silicate subsamples, totalling ~1.43 g)													
60635_A1	0.1698	1.213	1.232	13.52	14.0	21.2	29.4	18.3	0.12930	±7	0.432		0.432
60635_A2	0.0934	1.374	1.432	15.51	15.7	24.8	35.4	18.5	0.12975	±18	0.440		0.437
60635_A3	0.1741	1.360	1.416	15.40	14.8	26.3	32.5	21.4	0.12960	±15	0.425		0.436
60635_B1	0.1966	0.973	1.057	11.02	10.7	17.6	23.2	n.d.	n.d.		0.425		0.400
60635_B2	0.1441	0.836	1.009	9.416	9.40	15.2	19.3	12.9	0.12970	±23	0.428		0.437
60635_B3	0.1865	0.913	1.015	10.11	9.80	16.4	20.5	9.70	0.13278	±29	0.435		0.476
60635_B4	0.1512	0.929	0.952	10.57	11.0	17.3	20.9	10.4	0.12891	±15	0.424		0.427
60635_C	0.1222	0.927	0.945	10.47	11.3	17.2	20.7	14.2	0.12898	±18	0.427		0.428
60635_D1	0.1019	0.831	0.906	9.391	9.93	15.9	18.0	10.5	0.13129	±78	0.426		0.457
60635_D2	0.0903	1.844	1.961	21.21	21.9	35.6	41.0	28.1	0.12981	±23	0.419		0.438
average		1.063	1.131	11.97	12.4	20.1	25.4	15.5	0.1297	±9	0.428		0.437
Apollo 16 melt breccia 62295,18 (9 silicate subsamples, totalling ~0.90 g)													
62295_A	0.0884	0.394	0.382	3.649	3.85	8.58	11.63	12.31	0.13433	±15	0.520		0.495
62295_B1	0.1283	0.373	0.357	3.604	3.75	7.82	10.67	8.94	0.13232	±17	0.499		0.470

Sample	Wt. (g)	Re_{meas}	Re*calc[a]	Os	Ir	Ru	Pt	Pd	$^{187}Os/^{188}Os \pm 2\sigma$[b]		$^{187}Re/^{188}Os_{meas} \pm 2\sigma$[b]		$^{187}Re/^{188}Os_{calc}$
62295_B2	0.0754	0.492	0.478	4.571	4.73	9.74	14.29	11.09	0.13436	±22	0.519		0.496
62295_B3	0.0772	0.324	0.375	3.031	3.20	6.95	10.07	8.77	n.d.		0.515		
62295_C1	0.1027	n.d.	0.341	3.290	3.53	7.23	10.60	9.05	0.13398	±22	2.844		0.491
62295_C2	0.1165	0.796	1.042	6.857	7.25	15.54	20.59	18.97	0.13573	±22	0.559		0.513
62295_C3	0.0955	0.149	0.124	1.202	1.38	2.85	5.51	3.54	0.13427	±32	0.599		0.495
62295_C4	0.1235	3.266	3.166	28.46	29.35	59.53	80.46	67.76	0.13682	±13	0.553		0.527
62295_C5	0.0912	0.411	0.404	3.958	4.20	8.60	11.78	11.62	0.13289	±24	0.501		0.477
average	0.8988	0.870	0.824	7.223	7.54	15.57	21.45	18.53	0.1343	±10	0.662		0.495
Apollo 16 impact melt 63549,33 (9 silicate subsamples, totalling ~0.69 g)													
63549_A1	0.1127	n.d.	0.786	8.531	8.62	14.31	17.20	20.00	0.12971	±23	0.977		0.437
63549_A2	0.0729	n.d.	0.833	9.295	9.46	14.68	19.07	16.16	0.12878	±18	2.173		0.425
63549_B1	0.1023	0.715	0.766	8.337	8.06	13.68	16.88	17.59	0.12961	±15	0.413		0.436
63549_B2	0.0807	0.707	0.749	8.156	8.12	13.34	16.89	16.11	0.12960	±10	0.418		0.436
63549_B3	0.0722	0.766	0.836	9.073	8.88	14.42	21.36	17.43	0.12973	±18	0.407		0.437
63549_B4	0.0503	n.d.	0.733	8.184	8.21	13.16	21.24	15.13	0.12874	±69	0.891		0.425
63549_C1	0.0758	1.071	1.131	12.056	12.35	20.20	26.88	22.03	0.13032	±18	0.428		0.445
63549_C2	0.0718	0.750	0.884	8.656	8.15	14.64	n.d.	12.77	0.13344	±26	0.417		0.484
63549_C3	0.0523	0.959	0.981	10.437	10.03	17.65	23.09	26.19	0.13040	±18	0.443		0.446
average		0.819	0.814	9.114	9.03	15.00	17.76	18.10	0.1300	±9	0.725		0.441
Apollo 16 ancient regolith breccia Clast 65095,106b (8 subsamples, totaling ~0.201 g)													
65095_A1	0.0385	4.394	4.348	38.13	38.1	81.5	106.0	84.6	0.13785	±7	0.556	±4	0.539
65095_B1	0.0346	1.805	1.696	14.89	14.6	34.8	43.6	39.9	0.13781	±10	0.585	±9	0.539
65095_C1	0.0406	2.549	2.466	21.23	22.6	51.7	63.1	65.8	0.13864	±6	0.580	±6	0.549
65095_A1	0.0152	6.146	6.427	58.09	60.7	110	169	104	0.13658	±6	0.510	±5	0.523
65095_B1	0.0240	2.918	3.032	27.58	29.1	54.4	81.6	56.7	0.13632	±6	0.510	±7	0.520
65095_C1	0.0199	1.411	1.364	11.46	12.3	29.5	62.5	36.0	0.13972	±10	0.595	±20	0.563
65095_D	0.0142	0.680	0.567	4.384	5.23	17.2	25.4	25.0	0.14353	±15	0.749	±53	0.611
65095_C2	0.0142	0.891	0.800	6.218	7.20	21.7	47.6	29.3	0.14328	±11	0.692	±48	0.608
Average		2.71	2.67	23.50	24.5	52.5	74.3	58.4	0.1392	±20	0.597	±59	0.556
Apollo 16 basaltic impact melt breccia 67095,125 (10 silicate subsamples and 5 metal globules, totaling ~1.20 g)													
67095_B1	0.1120	0.244	0.250	2.361	2.45	4.26	6.10	4.58	0.13482	±8	0.499	±16	0.501
67095_B2	0.1672	0.128	0.130	1.198	1.25	2.54	3.27	3.22	0.13570	±10	0.516	±21	0.512
67095_C1	0.1678	0.179	0.187	1.778	1.88	3.97	5.13	4.35	0.13464	±7	0.486	±14	0.498
67095_D1	0.1625	0.270	0.279	2.618	2.73	5.41	7.17	5.68	0.13501	±7	0.497	±10	0.503
67095_E1	0.0975	0.260	0.271	2.579	2.68	5.30	6.90	5.36	0.13456	±8	0.486	±17	0.497
67095_B3	0.0865	0.383	0.378	3.323	3.49	7.33	9.21	8.75	0.13770	±6	0.539	±15	0.537
67095_B4	0.0790	0.154	0.146	1.363	1.47	2.96	3.61	3.78	0.13536	±14	0.503	±39	0.507
67095_C2	0.1308	0.106	0.105	1.015	1.10	2.20	2.79	2.21	0.13386	±11	0.469	±31	0.488
67095_D2	0.1156	0.172	0.168	1.643	1.74	3.51	4.24	3.65	0.13337	±6	0.481	±22	0.482
67095_E2	0.0851	0.706	0.723	6.935	7.16	13.6	17.3	13.4	0.13419	±6	0.483	±7	0.493

Sample	Wt. (g)	Re_{meas}	Re*calc[a]	Os	Ir	Ru	Pt	Pd	$^{187}Os/^{188}Os \pm 2\sigma$[b]		$^{187}Re/^{188}Os_{meas} \pm 2\sigma$[b]		$^{187}Re/^{188}Os_{calc}$
Metals													
67095_M1	0.000222	159	158	1439	1511	2840	4161	3222	0.13613	±5	0.532	±14	0.517
67095_M3	0.001453	29.5	29.6	275	284	567	1051	590	0.13547	±9	0.517	±11	0.509
67095_M4	0.000168	140	136	1118	1165	2371	3368	3026	0.14056	±10	0.603	±24	0.573
67095_M9	0.000057	186	208	1965	1775	3532	5028	3667	0.13480	±9	0.517	±39	0.500
67095_M10	0.000133	170	160	1412	1458	2972	3793	3353	0.13771	±6	0.582	±24	0.537
Average		0.35	0.35	3.28	3.41	6.74	10.0	7.37	0.1356	±10	0.514	±20	0.527
Apollo 16 impact melt 68416,16 (10 silicate subsamples, totaling ~0.80 g)													
68416_A1	0.0865	0.363	0.356	3.737	3.79	7.04	8.47	5.42	0.13080	±10	0.469	±14	0.450
68416_B1	0.0839	0.311	0.306	3.372	3.40	5.80	8.40	4.30	0.12912	±9	0.445	±15	0.428
68416_C1	0.0776	0.350	0.335	3.693	3.78	6.48	7.76	4.72	0.12919	±9	0.456	±16	0.429
68416_D1	0.0923	0.464	0.446	4.910	5.03	8.60	11.45	6.32	0.12919	±8	0.455	±10	0.429
68416_A2	0.0681	1.039	1.062	11.33	11.7	19.9	33.0	15.9	0.13028	±6	0.442	±6	0.443
68416_B2	0.0808	0.323	0.326	3.675	3.73	6.18	8.47	3.10	0.12837	±7	0.424	±15	0.419
68416_C2	0.0811	0.303	0.311	3.434	3.57	6.00	8.71	3.34	0.12914	±8	0.426	±15	0.429
68416_D2	0.0813	1.275	1.279	13.83	14.0	23.5	31.9	18.4	0.12981	±7	0.444	±4	0.437
68416_E	0.0679	0.381	0.385	4.203	4.31	7.32	12.68	4.18	0.12946	±8	0.437	±16	0.433
68416_F1	0.0838	1.489	1.493	15.50	16.3	28.3	37.0	24.0	0.13124	±6	0.463	±4	0.455
Average	0.8032	0.63	0.63	6.72	6.91	11.84	16.54	8.93	0.1297	±6	0.446	±9	0.435

Estimated uncertainties for concentration data are on average better than 0.5 % for Os and Ir, 1 % for Ir, Pt and Pd, and 5 % for Re.

[a] Re*calc represents calculated Re concentrations as stated in text, so forth $^{187}Re/^{188}Os_{calc}$ versus $^{187}Re/^{188}Os_{meas}$.

[b] Errors in $^{187}Os/^{188}Os$ and $^{187}Re/^{188}Os_{meas}$ of subsamples of a given impact rock are shown as $\pm 2\sigma$ and refer to the last decimal places (Errors for $^{187}Re/^{188}Os_{meas}$ were estimated assuming 100 % variation in the blank contribution).

[c] Mass-weighted averages for the concentration data, and simple averages ($\pm 2\sigma_{mean}$) for $^{187}Os/^{188}Os$.

Table 3.

Slopes and intercepts of Ir versus HSE trends, as well as simple ratio averages, for the lunar melt rocks

Samples	**15445**	**15455**	**60016,286b**		**60016,290b**			**60235**	
Intercepts	**silicate**	**silicate**	**silicate**	**silicate**	**silicate**	**silicate+metal**	**silicate+metal**	**silicate**	**silicate**
ng/g	***regression***	***regression***	***regression***	***average***	***regression***	***regression***	***average***	***regression***	***average***
Re	−0.02±0.11	0.005±0.072	0.23±0.25		0.46±0.59	0.08±0.19		0.15±0.16	
Re*	0.17±0.69	−0.015±0.035	0.12±0.12		0±0.6	0.11±0.09		0.006±0.081	
Os	−0.25±0.79	−0.01±0.18	1.9±1.6		−1.2±3.1	0.7±3.3		0.17±0.69	
Ru	−0.01±0.78	0.01±0.84	6.6±3.2		3±20	3.1±4.5		1.0±1.3	
Pt	0±1.8	0.3±1.0	6±21		−21±39	1±72		3.9±2.1	
Pd	1.1±2.0	1.5±1.5	13.6±6.4		3±38	8±68		3.0±2.4	
Slopes/Average Ratios									
Re/Ir	0.106±0.019	0.104±0.014	0.093±0.020	0.111±0.004	0.092±0.026	0.109±0.008	0.113±0.004	0.094±0.022	0.118±0.031
Re*/Ir	0.108±0.017	0.106±0.007	0.099±0.010	0.108±0.002	0.110±0.027	0.105±0.0002	0.109±0.003	0.104±0.011	0.104±0.013
Os/Ir	1.00±0.14	0.922±0.031	0.79±0.11	0.946±0.031	0.99±0.13	0.905±0.008	0.932±0.014	0.926±0.095	0.942±0.114
Ru/Ir	2.17±0.14	2.31±0.15	1.85±0.22	2.40±0.08	2.28±0.84	2.27±0.01	2.38±0.08	1.92±0.18	2.04±0.20
Pt/Ir	2.55±0.31	2.59±0.18	2.5±1.6	3.04±0.14	3.9±1.6	2.98±0.17	3.02±0.15	2.14±0.28	2.67±0.29
Pd/Ir	2.06±0.35	2.26±0.27	1.92±0.45	3.04±0.17	3.1±1.6	2.84±0.16	3.15±0.17	2.00±0.33	2.43±0.49
$^{187}Os/^{188}Os$	0.1348±7	0.1372±4	0.1383±10			0.1390±8			0.1362±7
Samples	**60635**	**62295**	**63549**	**65095**			**67095**		**68416**
Intercepts	**silicate**	**silicate**	**silicate**	**silicate**	**silicate**	**silicate**	**silicate+metal**	**metal**	**silicate**
ng/g	***regression***	***regression***	***regression***	***regression***	***average***	***regression***	***regression***	***regression***	***regression***
Re	0.04±0.11	−0.029±0.029	0.002±0.23	0.15±0.07		−0.002±0.014	−0.012±0.009	−2.1±4.1	−0.004±0.032
Re*	0.10±0.19	−0.005±0.096	0.02±0.28	0.01±0.07		−0.008±0.007	−0.3±3.0	−4±34	−0.011±0.016
Os	0.1±1.2	−0.11±0.05	0.8±1.3	−0.4±1.2		−0.047±0.028	−7±39	−94±430	0.07±0.17
Ru	0.7±2.7	0.35±0.30	0±3.7	9.4±5.8		0.18±0.39	1±34	17±400	0±0.4
Pt	−0.2±5.9	1.14±0.43	−3±12	17±15		0.32±0.39	18±73	278±680	0±2.9
Pd	−3.8±5.2	1.5±1.1	−10±21	19±11		0.69±0.94	6±100	105±1100	−1.5±1.2
Slopes/Average Ratios									
Re/Ir	0.084±0.009	0.112±0.003	0.089±0.025	0.103±0.006	0.115±0.007	0.101±0.008	0.107±0.004	0.112±0.007	0.091±0.007
Re*/Ir	0.085±0.014	0.110±0.009	0.092±0.031	0.109±0.006	0.110±0.003	0.105±0.004	0.112±0.004	0.115±0.02	0.092±0.004
Os/Ir	0.975±0.090	0.973±0.005	0.92±0.14	0.975±0.041	0.937±0.043	0.974±0.009	1.019±0.050	1.08±0.32	0.963±0.020
Ru/Ir	1.67±0.20	2.02±0.03	1.66±0.41	1.72±0.20	2.40±0.37	1.90±0.13	1.98±0.04	1.97±0.30	1.71±0.05
Pt/Ir	2.04±0.44	2.70±0.04	2.6±1.3	2.43±0.53	3.44±0.75	2.41±0.13	2.77±0.09	2.59±0.50	2.41±0.35
Pd/Ir	1.51±0.38	2.27±0.10	3.0±2.3	1.51±0.36	2.91±0.74	1.85±0.31	2.22±0.13	2.15±0.85	1.51±0.14
$^{187}Os/^{188}Os$	0.1297±10	0.1343±10	0.1300±9	0.1392±20		0.1349±8	0.1356±10	0.1369±21	0.1297±6

Note: “silicate” represents bulk silicate subsamples, “metal” represents individual metals, “regression” means values from the trends of lr versus HSE, and “average” means simple average ratios of the subsamples of each rock. All errors are given in 2σ.

Table 4.

Siderophile element concentrations (μg/g) of lunar metal and troilite grains determined by laser ablation ICP-MS

Eelement	Cr	Fe (%)	Co	Ni (%)	Zn	Ga	Ge	Ru	Rh	Pd	Re	Os	Ir	Pt	Au
Metals															
M1 rim	bdl	89.9	2769	9.85	bdl	0.34	0.16	3.59	0.60	3.44	0.07	0.56	0.61	1.75	0.79
M1 core	bdl	94.7	4046	4.92	0.19	0.71	0.31	2.73	0.55	2.35	0.20	1.84	1.88	4.66	1.84
M3	29	85.0	1694	14.9	0.42	2.47	0.32	4.71	0.57	5.52	0.06	0.55	0.60	1.45	0.44
M6 rim	24	86.4	1361	13.5	0.47	0.41	0.05	5.44	0.76	4.56	0.04	0.13	0.07	0.21	bdl
M6 core	bdl	95.4	3942	4.17	bdl	1.61	0.36	3.27	0.80	3.42	0.20	2.25	2.35	6.17	2.07
M9	bdl	96.8	4319	2.78	0.41	1.12	0.43	3.14	0.73	2.81	0.26	2.42	2.47	6.46	1.86
M10	11	86.9	1412	13.0	0.38	0.20	0.08	4.38	0.58	4.25	bdl	0.14	0.13	0.31	0.16
M11-1	11	96.5	2562	3.23	bdl	1.21	0.53	0.14	0.02	0.31	bdl	0.02	0.01	bdl	0.95
M11-2	bdl	96.6	2512	3.16	bdl	1.21	0.50	bdl	bdl	0.36	0.08	bdl	bdl	bdl	0.97
Troilites															
M2	44	60	bdl	0.04	0.68	bdl	0.03	bdl	bdl	bdl	bdl	bdl	bdl	bdl	bdl
M5	31	60	bdl	0.02	0.83	0.05	0.03	bdl	0.03	bdl	bdl	bdl	bdl	bdl	bdl
M7	29	60	bdl	0.01	0.78	0.66	0.04	bdl	bdl	bdl	bdl	bdl	bdl	bdl	bdl
M8	48	60	bdl	0.02	0.75	1.15	0.03	bdl	bdl	bdl	bdl	bdl	bdl	bdl	bdl
M12	40	60	bdl	0.01	0.68	bdl	0.04	bdl	bdl	bdl	bdl	bdl	bdl	bdl	bdl
M13	52	60	bdl	0.02	0.70	bdl	0.04	bdl	bdl	bdl	bdl	bdl	bdl	bdl	bdl
Dection limit	1	0.01	3	0.001	0.04	0.02	0.01	0.03	0.01	0.02	0.004	0.01	0.01	0.03	0.02

bdl: below detection limit; rim: the first ablation analysis; core: the second albation analysis on the same spot as the first ablation For troilites, an assumed Fe content of 60 % is set as the internal standard.

Table 5.

Calculated bulk siderophile element concentrations (μg/g) of 67095 grain M1

Element	Cr	Fe (%)	Co	Ni (%)	Zn	Ga	Ge	Ru	Rh	Pd	Sb	Re	Os	Ir	Pt	Au
M1 rim[a]	bdl	89.9	2769	9.85	0	0.34	0.16	3.59	0.60	3.95	0	0.07	0.56	0.61	1.75	0.79
M1 core[a]	bdl	94.7	4046	4.92	0.19	0.71	0.31	2.73	0.55	2.55	1.62	0.20	1.84	1.88	4.66	1.84
M1 bulk calc	-	93.3	3674	6.35	0.13	0.60	0.27	2.98	0.57	2.96	1.15	0.16	1.47	1.51	3.81	1.53
M1 bulk id[b]	-							2.84		3.22		0.16	1.44	1.51	4.16	

Note: The bulk siderophile element concentrations are calculated via mixing of rim and core with a certain proportion (roungly 1:9 in thickness for M1 assumed as an ideal spherical globule) that meets the bulk Ir concentration determined using isotope dilution. The calculated HSE concentrations are in less than 10 % differences from the bulk isotope dilution values.

[a] laser ablation data from Table 4.

[b] bulk isotope dilution data from Table 2.